THE ASTROPHYSICAL JOURNAL, 431:515–533, 1994 August 20

THE COMPLEX OPTICAL TO SOFT X-RAY SPECTRUM OF THE LOW-REDSHIFT RADIO-QUIET QUASARS. I. THE X-RAY DATA

FABRIZIO FIORE,[1] MARTIN ELVIS, JONATHAN C. MCDOWELL, ANETA SIEMIGINOWSKA, AND BELINDA J. WILKES
Harvard-Smithsonian Center for Astrophysics, 60 Garden Street, Cambridge MA 02138
Received 1993 December 3; accepted 1994 February 23

ABSTRACT

Eight high signal-to-noise *ROSAT* PSPC observations of six low-redshift ($0.048 < z < 0.155$) radio-quiet quasars have been analyzed to study any soft excess. All the spectra can, at least roughly, be described in the 0.1–2.5 keV band by simple power laws reduced at low energies by Galactic absorption. The strong oxygen edges seen in the PSPC spectra of several Seyfert galaxies and quasars are not observed in this sample. The limits implied for the amount of absorbing gas intrinsic to the quasars are particularly tight: of the order of $\sim 10^{20}$ cm^{-2}. The range of energy indices is broad: $1.3 < \alpha_E < 2.3$. The energy indices are systematically steeper than those found in the same sources at higher energies [by $\Delta\alpha_E \sim 0.5$–1 with respect to *Ginga* or *EXOSAT* (2–10 keV) measurements, and by $\Delta\alpha_E \sim 0.5$ with respect to IPC (0.2–3.5 keV) measurements]. This suggests a break between the hard and soft components in the "keV" region and, therefore, that the PSPC spectra are strongly dominated by the soft components. In fact, a fit to the composite, high signal-to-noise spectrum reveals a significant excess above ~ 1 keV with respect to the simple power-law model. No evidence for strong emission lines is found in any of the quasars. This argues against emission from an ionized plasma as the main contributor to the soft X-ray component unless there is a distribution of temperatures. If the soft X-ray spectrum of these quasars is dominated by radiation reflected by the photoionized surface of an accretion disk, the absence of strong emission lines suggests high ionization parameters and therefore high accretion rates.

We include in two Appendices a comparison of the two official PSPC resolution matrices, those released on 1992 March and on 1993 January, a discussion of the amplitude of the residual systematic uncertainties in the 1993 January matrix, and a comparison between the PSPC and IPC spectra of a sample of sources.

Subject headings: quasars: general — X-rays: galaxies

1. INTRODUCTION

The *Einstein* IPC and MPC and the *EXOSAT* CMA and ME observations of Active Galactic Nuclei (AGNs) uncovered an unexpected complexity in AGN soft X-ray spectral shapes. The single power-law model with Galactic or intrinsic absorption is in many cases an inadequate description of the 0.2–10 keV spectrum. About 50% of luminous quasars (Wilkes & Elvis 1987; Masnou et al. 1992) and of Seyfert galaxies (Turner & Pounds 1989 and references therein) show some sort of "soft excess" above the extrapolation in the 0.1–2 keV band of the 2–10 keV power law.

So far, several types of soft excess have been suggested to exist in AGNs:

1. A steep, constant excess associated with extended emission around the active nucleus (e.g., NGC 4151, Elvis et al. 1990 and Perola et al. 1986; NGC 1068, Wilson et al. 1992), visible when the central X-ray source is obscured by dense gas.
2. Excess emission in the 0.5–2 keV band possibly due to leakage of the hard power law through a "partial covering" absorber (e.g., NGC 4151; see Yaqoob & Warwick 1991 and references therein).
3. The recovery of the spectrum below the oxygen edge in "warm absorber" sources (e.g., MGC −6-30-15, Nandra & Pounds 1992; 3C 351, Fiore et al. 1993; NGC 3783, Turner et al. 1993c).
4. Emission line features in the 0.7–1 keV band (Turner et al. 1991).
5. A steep, broadband and variable excess.

Such steep and broad soft X-ray excesses have been interpreted in terms of:

1. Optically thick emission from the inner edge of an accretion disk (e.g., MKN 335, Turner & Pounds 1988; PG 1211+143, Elvis et al. 1991).
2. Reprocessing from optically thick gas surrounding the hard X-ray source (Guilbert & Rees 1988; Lightman & White 1988; Ross & Fabian 1993).
3. Optically thin free-free emission from gas with temperature the order of 10^6 K (Barvainis 1993).
4. Pair cascade models, due to upscattering of the UV photons by thermalized pairs (MKN 335, Turner et al. 1993).

The discovery by *Ginga* of a new hard component in AGN spectra (Pounds et al. 1990; Piro, Yamauchi, & Matsuoka 1990) complicates further this already crowded picture. On the one hand, the interpretation of this component and of the iron K lines seen in most Seyfert galaxies in terms of reprocessing of the primary continuum (Guilbert & Rees 1988; Lightman & White 1988) gives support to the idea that optically thick gas surrounds the central X-ray source. This optically thick gas can be identified with that responsible for the emission of the steep and variable soft component. On the other hand, when the *Ginga* spectra are fitted with a two-component model, the primary power law, and the reprocessed continuum, the energy slope of the first is about 1, steeper by $\Delta\alpha_E \approx 0.3$ than the value

[1] Postal address: Osservatorio Astronomico di Roma, via dell'Osservatorio 5, Monteporzio-Catone (Rome), I-00040, Italy.

obtained adopting a single power-law model. Neglecting the reprocessed continuum in IPC/MPC and *EXOSAT* ME/LE fits inevitably results in an apparent excess of soft photons, since the intensity of the reprocessed continuum falls rapidly below 5 keV (unless the gas is significantly ionized).

Since most observations were made with instruments of limited sensitivity below 0.5 keV and/or limited energy resolution, it has been impossible to discriminate unambiguously among the different possibilities. Therefore, some of the "soft excess" may not necessarily indicate the existence of a separate soft component but could simply result from the assumption of the wrong absorption model or the wrong emission model above 2 keV. Moreover, even where the evidence for a soft excess is stronger, very little is known about its shape.

The *ROSAT* (Trümper 1983) PSPC (Pfeffermann et al. 1987), with its good sensitivity between 0.1 and 2 keV and better energy resolution (40% FWHM at 1 keV) in comparison with the IPC and the *EXOSAT* LE, is a better tool to study the complex soft X-ray spectrum of AGNs than was previously available. In particular, the PSPC can be used to try to distinguish between different types of soft excess. For this reason, we observed with the PSPC six low-redshift, radio-quiet quasars, selected to be among the brightest with known soft excesses. Our aim was to obtain high signal-to-noise detections ($\gtrsim 100\ \sigma$) to allow the extraction of the maximum spectral information. As a result, it becomes worthwhile to investigate a wider range of spectral forms than has been reasonable before with quasar X-ray spectra. In the following we present the analysis of the quasar's integrated spectra. The analysis of the quasars' temporal variations is in progress and will be part of a follow-up paper. The implications of the results reported in this paper for models of quasars where the soft X-ray excess and the big blue bump are interpreted in terms of (1) free-free emission from optically thin plasma, and (2) optically thick thermal emission from the innermost region of an accretion disk, are presented and discussed in detail in a companion paper (Fiore et al. 1994).

2. OBSERVATIONS AND DATA ANALYSIS

The six quasars were observed by *ROSAT* between 1990 July and 1992 January. Two objects were observed twice at 6 month intervals. Seven observations were performed with the PSPC-B in the focal plane, while that of PG 1426+0.15 was performed with the PSPC-C during the performance verification (PV) phase. Some results from the latter observation have been already presented by Fiore et al. (1993). During all observations the standard wobble mode was on, moving the telescope pointing direction to and fro along a 3′ path with a ~400 s period, to smooth out the effect of the detector structure. The data were processed using the Standard Analysis Software System (SASS), and the number of the SASS version used in each observation is given in Table 1 together with the observation date, the observation time and the net counts (pulse invariant [PI] channels 11–245, ≈0.11–2.45 keV) within a circle of radius 3′ around the X-ray centroid of the source. This rather large radius was chosen to collect as many soft photons in the so-called electronic ghost images as possible, while still retaining a reasonably low background. The "electronic ghost images" form at low energies, below ~0.2 keV (Hasinger et al. 1992), and are present in all but the PG 1426+0.15 observations, i.e., in all observations performed with the PSPC-B. The background spectra were taken from annuli of inner and outer radii between 3′.5 and 7′. The source counts in the entire energy band and in the soft (PI 11–40 ≈ 0.1–0.4 keV) energy band do not increase significantly when broader source and background regions are used, suggesting that most of the source counts lie within 3′.

In Table 1 we give also the source count rate corrected for the dead time (using the standard correction factor of 1.03) for each observation. We evaluated at about 4% the systematic error on the count rate (and therefore on the flux) due to the combined uncertainty in the dead time correction (±1%–2%, i.e., 1.03 ± 0.01–0.02; L. David 1993, private communication); in local variations in the PSPC quantum efficiency; and to the obscuration of the PSPC window supporting structure (at the center of the field, where all our sources are located, the effective exposure time is typically within ±2% of the observation time). This systematic error has been added in quadrature to the statistical error and dominates the error on the count rate in Table 1.

The 34 energy channels from the MPE SASS pipeline processing were used in the spectral analysis. The spectra were compared to various trial models employing the most recent official response matrix, that released in 1993 January. An exception is PG 1426+015, for which we present the results obtained with the 1992 March response matrix. A comparison between the two resolution matrices is presented in Appendix A, together with a discussion of the reliability of the PSPC calibrations. The first two channels were always excluded from the analysis, and therefore the fits were performed in the 0.11–2.45 keV band (channels 3–34).

TABLE 1

ROSAT PSPC OBSERVATIONS OF QUASARS

Name	z	Exposure[a]	Net Counts[b]	Count Rate[c]	IPC count rate[c,d]	$N_{HGal}^{e,f}$	Date	SASS
NAB 0205+024	0.155	14070	9382	0.687 ± 0.028	0.18 ± 0.01	2.99	1992 Jan 18-23	5.6
PG 1211+143	0.085	3877	3803	1.010 ± 0.042	1.22 ± 0.03	2.83	1991 Dec 17-24	5.6
MKN 205 (11/91)	0.07	6398	8176	1.316 ± 0.053	0.49 ± 0.01	2.74	1991 Nov 10-12	5.6
MKN 205 (4/92)		7493	5568	0.765 ± 0.031			1992 Apr 15	5.7
TON 1542(12/91)	0.064	6183	7734	1.288 ± 0.052	0.22 ± 0.01	2.58	1991 Dec 13-26	5.6
TON 1542(7/92)		5816	7617	1.349 ± 0.055			1992 Jul 6	5.7
PG 1244+026	0.048	5566	5509	1.020 ± 0.042	0.33 ± 0.02	1.93	1991 Dec 22-24	5.6
PG 1426+015	0.086	6485	9689	1.538 ± 0.062	0.50 ± 0.01	2.64	1991 Jul 18-19	5.3.2

[a] In seconds.
[b] In 3′ circles.
[c] In counts s^{-1}.
[d] Harris et al. 1990.
[e] In units of 10^{20} cm^{-1}.
[f] Elvis, Lockman, & Wilkes 1989.

TABLE 2

ROSAT PSPC OBSERVATIONS WITH THE BORON FILTER

Name	Exposure[a]	Net Counts[b]	Count Rate[c]	Date	SASS
NAB 0205+024	7835	968	0.12 ± 0.01	1992 Jan 23-24	5_6
PG 1211+143	3119	634	0.20 ± 0.01	1991 Dec 25	5_6
MKN 205 (11/91)	1587	797	0.50 ± 0.02	1991 Nov 11	5_7
MKN 205 (4/92)	2358	714	0.30 ± 0.02	1992 Apr 15	5_7
PG 1244+026	3155	237	0.08 ± 0.01	1991 Dec 24	5_7
PG 1426+015	5998	3166	0.53 ± 0.02	1990 Jul 19	5_3_2

[a] In seconds.
[b] In 3′ circles.
[c] In counts s^{-2}.

2.1. *PSPC Observations with the Boron Filter*

We also observed five of the six quasars with the *ROSAT* PSPC covered with the boron filter (Stephan et al. 1991). Since the boron filter supresses the radiation between 0.188 keV and 0.28 keV its use can improve the spectral resolution at the low-energy end of the PSPC band by comparing measurements with and without the filter. Table 2 gives the exposure time, the net counts within a circle of 3′ radius (PI channels 11–245), the observation date and the SASS version for each observation.

3. RESULTS

3.1. *Simple Power-Law Fits*

The results of fitting a power law with low-energy neutral and uniform absorption (using the atomic cross-sections from Morrison & McCammon 1983), hereafter the PL model, are given in Table 3, columns (2)–(6). Errors represent the 68% confidence interval for two interesting parameters (Lampton, Margon, & Bowyer 1976). We also list in the same Table, columns (7)–(9), results from previous experiments: *Einstein*

TABLE 3

POWER-LAW SPECTRAL FITS

		ROSAT	PSPC			*Einstein*	IPC	2-10 keV
Name	Norm.[a]	α_E	N_H^b	$\chi^2(dof)$	Prob. %	α_E	N_H^e	α_E
NAB0205+024	1.16 ± 0.04	2.26 ± 0.10	3.41 ± 0.25	34.70 (27)	14.7	$1.2^{+0.6}_{-0.10}$ [c]	$0.8^{+2.5}_{-0.3} + 3$	1.2[d]
$E > 0.5$ keV	1.16 ± 0.03	2.18 ± 0.07	2.99FIXED	23.65 (18)	16.7			
PG1211+143	2.05 ± 0.09	2.00 ± 0.14	3.25 ± 0.36	39.64 (27)	5.5	$1.8^{+0.5}_{-0.4}$[c]	$2.1^{+1.9}_{-1.3}$	$1.11^{+0.17}_{-0.13}$[e]
$E > 0.5$ keV	2.03 ± 0.06	1.90 ± 0.10	2.83FIXED	29.66 (18)	4.0			
MKN205-tot.	3.32 ± 0.06	1.36 ± 0.06	3.30 ± 0.19	31.43 (29)	34.5	0.8 ± 0.2[c]	2.0 ± 0.9	$0.91^{+0.09}_{-0.08}$[e]
$E > 0.5$ keV	3.28 ± 0.04	1.28 ± 0.04	2.74FIXED	22.15 (20)	33.2			
MKN205 (11/91)	4.20 ± 0.10	1.38 ± 0.08	3.24 ± 0.24	29.48 (28)	38.8			
MKN205 (4/92)	2.55 ± 0.07	1.32 ± 0.10	3.32 ± 0.30	38.44 (28)	9.03			
TON 1542-tot.	2.24 ± 0.05	1.71 ± 0.06	2.02 ± 0.14	30.38 (28)	34.5	$1.5^{+0.2}_{-0.1}$[f]	2.58FIXED	$1.14^{+0.33}_{-0.31}$[g]
$E > 0.5$ keV	2.30 ± 0.04	1.66 ± 0.05	2.58FIXED	15.10 (19)	71.6			
TON 1542(12/91)	2.40 ± 0.07	1.61 ± 0.09	2.01 ± 0.19	19.92 (28)	86.7			
TON 1542(7/92)	2.06 ± 0.07	1.84 ± 0.09	2.08 ± 0.20	25.26 (28)	61.4			
PG1244+026	1.36 ± 0.06	2.31 ± 0.12	2.91 ± 0.28	22.84 (25)	58.7	$1.5^{+1.3}_{-0.5}$[h]	$1.0^{+5.0}_{-1.0}$	
$E > 0.5$ keV	1.33 ± 0.04	2.28 ± 0.09	1.93FIXED	16.05 (16)	44.9			
PG1426+015	3.83 ± 0.09	1.52 ± 0.07	2.55 ± 0.20	34.67 (29)	21.6	0.9 ± 0.2[c]	$1.3^{+1.4}_{-0.7}$	0.46 ± 0.25[g]
$E > 0.5$ keV	3.75 ± 0.07	1.49 ± 0.05	2.64FIXED	20.65 (20)	41.8			
soft-7[i]	2.13 ± 0.02	1.69 ± 0.04	2.58 ± 0.09	53.47 (29)	0.37			
soft-7-sim[j]	2.15 ± 0.02	1.69 ± 0.03	2.61 ± 0.09	28.00 (29)	51.8			

NOTES.—PSPC errors represent the 68% confidence for two interesting parameters. IPC *EXOSAT*, and *Ginga* errors represent the 90% confidence for two interesting parameters.
[a] Flux density in units of 10^{-3} cm^{-2} s^{-1} keV^{-1} at 1 keV.
[b] In units of 10^{20} cm^{-2}.
[c] Wilkes & Elvis 1987.
[d] Masnou et al. 1992.
[e] Williams et al. 1992.
[f] Shastri et al. 1993.
[g] Comastri et al. 1992.
[h] Elvis et al. 1986.
[i] Composite spectrum, obtained adding together the seven spectra of NAB 0205+024, PG 1211+143, MKN 205, TON 1542, and PG 1244+026.
[j] Simulated composite spectrum, obtained adding together the simulations of the seven spectra of the above five quasars obtained using the best-fit values in the table.

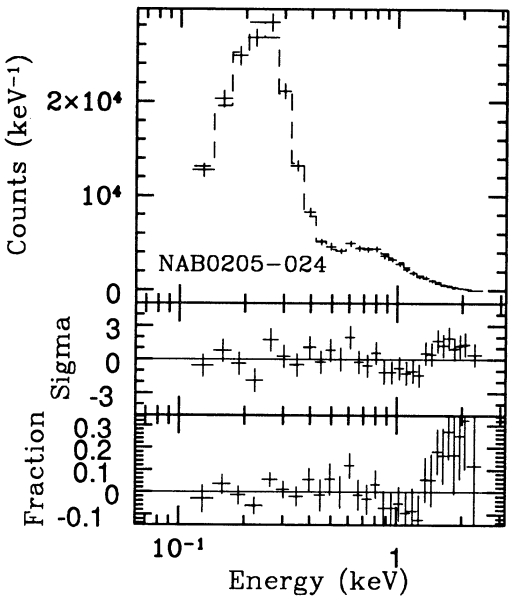

FIG. 1a

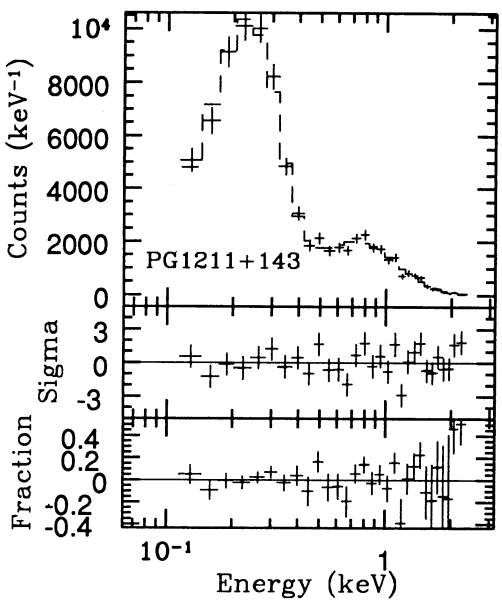

FIG. 1b

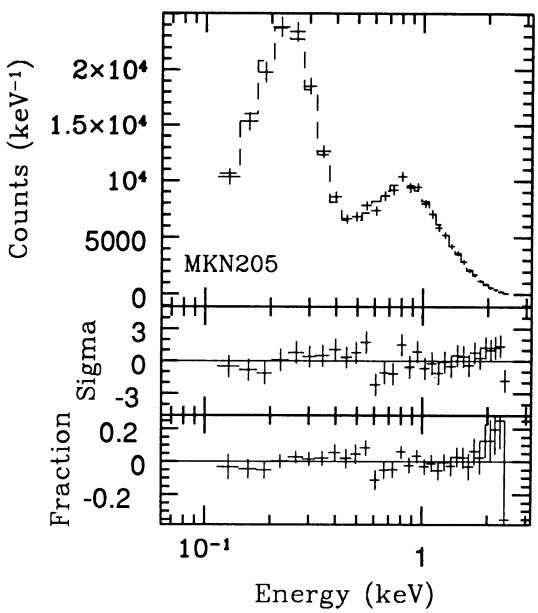

FIG. 1c

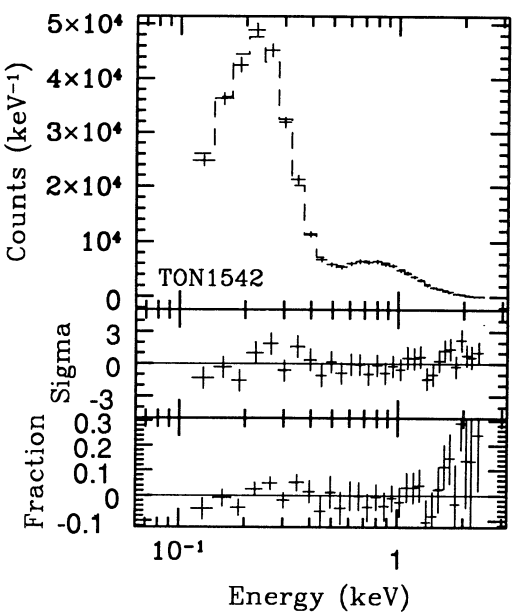

FIG. 1d

FIG. 1.—Single power law with low-energy absorption spectral fit to the spectra of (*a*) NAB 0205+024, (*b*) PG 1211+143, (*c*) MKN 205, (*d*) TON 1542, (*e*) PG 1244+0.26, and (*f*) PG 1426+015. Energies are in the observed frame.

IPC (0.1–3.5 keV) and MPC (2–6 keV), *EXOSAT* ME (1–8 keV), *Ginga* LAC (2–18 keV). The pairs of spectra for both MKN 205 and TON 1542 acquired 6 months apart are similar in shape, and in the following we also consider their co-added spectra. The spectra of the six quasars with the best fitting PL model are shown in Figures 1*a*–1*f*, upper panels. The lower panels show the residuals after the subtraction of the best fitting PL model from the data both as a number of σ and as a fraction of the counts in each channel. In Table 3 we also give the results of fitting the single PL model to the spectra of the six quasars only above 0.5 keV (channels 13–34). The N_H has been here fixed to the Galactic value, since letting it be free to vary does not significantly improve the fits.

The value of the χ^2 statistic listed in Table 3 suggests that the PL model is acceptable in most cases and therefore that the spectrum of these quasars is actually dominated by a single broad component in the 0.2–2 keV band. Fits with a blackbody or thermal bremsstrahlung models give much higher χ^2. The amplitude of any narrow feature is in all cases less than 10%–20% of the counts per channel.

The best fit for the column density N_H is the order of, or slightly higher than, the Galactic one in all quasars but TON 1542. In the latter case the $\Delta\chi^2$ obtained by fixing N_H to the Galactic value of 2.58×10^{20} atoms cm^{-2} (Elvis, Lockman, & Wilkes 1989) is 32.9, corresponding to a probability of $< 10^{-8}$.

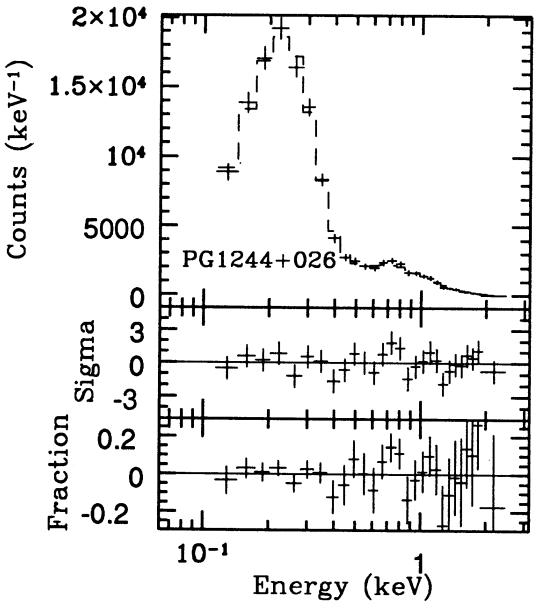

FIG. 1e

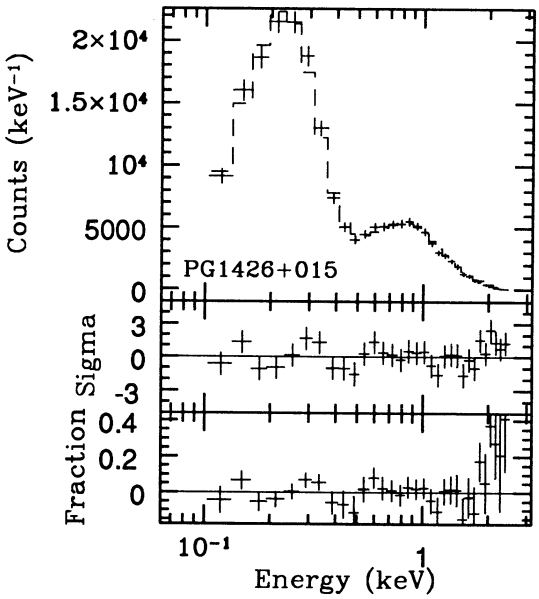

FIG. 1f

Fig. 1.—*Continued*

The 0.5–2.5 keV PSPC energy spectral indices [α_E, $f(E) \propto E^{-\alpha_E}$] are, within the errors, similar to the 0.1–2.5 PSPC energy indices. The average 0.1–2.5 energy index is $\langle \alpha_E \rangle = 1.68 \pm 0.03$, while the average 0.5–2.5 energy index is $\langle \alpha_E \rangle = 1.62 \pm 0.02$ (here and below, the quoted uncertainties on the mean slopes are the errors on the mean values).

The PSPC energy indices are systematically steeper than the 2–10 keV energy indices measured by *EXOSAT* or *Ginga*, $\Delta\alpha_E = 0.5$–1, (Fig. 2*a*). For example, the average 2–10 keV α_E found by Williams et al. (1992) in a sample of six radio-quiet quasars is $\langle \alpha_E \rangle = 1.04 \pm 0.05$, and the average 2–10 keV α_E of the four quasars in the present sample with high-energy observations is $\langle \alpha \rangle_E = 0.92 \pm 0.07$. This difference is much larger than the systematic error of ~ 0.2 on PSPC spectral indices evaluated in Appendix A.

Somewhat surprisingly, the PSPC α_E are also significantly steeper than the IPC spectral indices in three cases, with $\Delta\alpha_E = 0.5$–0.7, and the average IPC slope of the six quasars is $\langle \alpha_E \rangle = 1.18 \pm 0.10$, significantly flatter than both the overall and the 0.5–2.5 keV average PSPC spectral index. In Figure 2*b*, we plot the IPC and PSPC energy indices for the six quasars and those of the other quasars in common between the

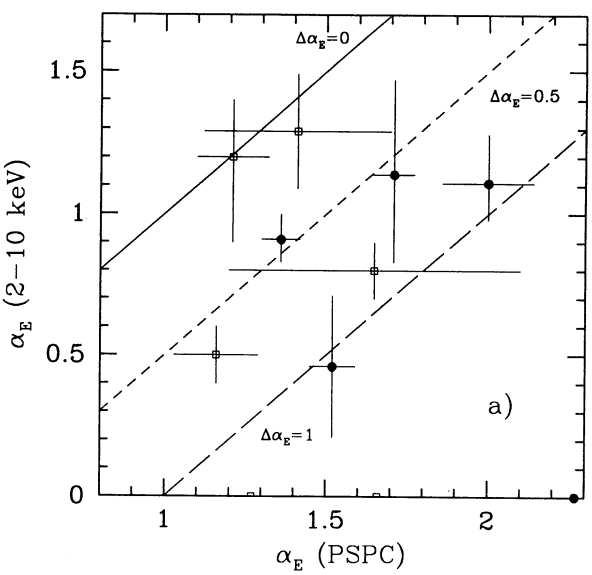

FIG. 2a

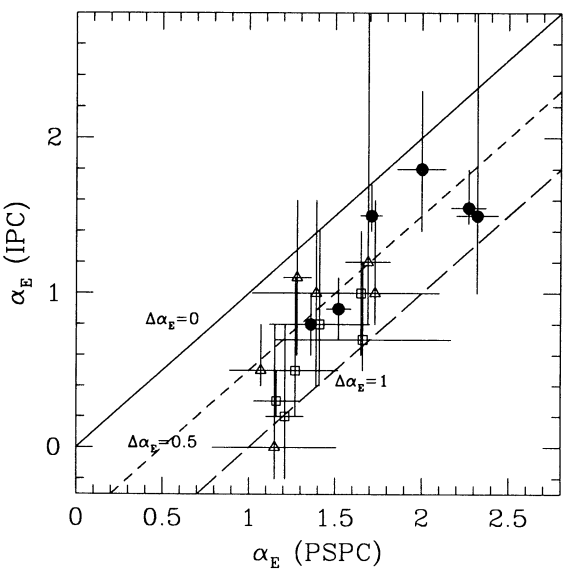

FIG. 2b

FIG. 2.—(*a*) The 0.1–2.5 PSPC spectral indices plotted against the 2–10 keV *EXOSAT* or *Ginga* spectral indices for PG 1211+143, MKN 205, TON 1542, and PG 1426+015. (*b*) The PSPC spectral indices plotted against the IPC spectral indices for the six quasars (*filled circles*). Open squares identify the quasars in common between the Wilkes & Elvis (1987) and Walter & Fink (1993) samples. Open triangles identify other quasars in the Wilkes & Elvis (1987) sample observed with the PSPC by our group for other projects.

samples of Wilkes & Elvis (1987) and Walter & Fink (1993) (*open squares*) and for other quasars in the sample of Wilkes & Elvis (1987) observed with the PSPC by our group in other projects (*open triangles*). It is apparent that the PSPC slopes of this sample of quasars (18 quasars in total) are systematically steeper than the IPC slopes and that the difference is not limited to the bright radio-quiet quasars discussed in this paper. A similar discrepancy between IPC and PSPC slopes has been pointed out also by Brunner et al. (1992) and Jackson, Browne, & Warwick (1993). We will further discuss the comparison between the PSPC and the IPC measurements in § 3.7 and in Appendix B. We note here that this discrepancy is larger than the systematic uncertainty on the PSPC spectral index evaluated in Appendix A.

The difference between the PSPC and the 2–10 keV spectral indices together with the fact the PSPC spectra are dominated by a single broad component suggest a complex soft X-ray spectrum with a sharp "break point" between the soft and hard spectra in the "keV" region. A break at this energy is also suggested by the Broad-Band X-Ray Telescope (BBXRT) observation of MKN 335 (Turner et al. 1993b). Unfortunately, above 1.5 keV the sensitivity of *ROSAT* falls rapidly (for example, we have only between 100 and 700 counts above 1.5 keV in each spectrum, always less than 1/10 of the total number of counts), preventing a detailed study of the break point in single spectra Nevertheless, the analysis of the residuals in Figure 1 indicates in some cases a small deficit of counts between 0.5 keV and 1 keV and an excess above 1.5 keV, which supports the above suggestion.

3.1.1. *Fitting the PSPC Boron Filter Data*

The results of fitting the PL model to the boron filter data are given in Table 4. The single χ^2 are all acceptable, but they are systematically higher than those obtained fitting the same model to the open PSPC data (Table 3). Since here the statistics are worse than in the previous case, this indicates that (1) the deviations of the real spectra from the PL model become more evident when improving the energy resolution; and/or (2) there are large systematic uncertainties in the knowledge of the filter transmission. The best-fit spectral indices are close to those found with the open PSPC ($\langle \alpha_E \rangle = 1.59 \pm 0.09$), while the best-fit N_H are systematically lower but still always compatible with the Galactic value along the line of sight (the only source with best-fit N_H significantly less than the Galactic value in the open PSPC, TON 1542, has not been observed with the boron filter). The residuals after subtracting the best fitting PL model show a systematic $\sim 50\%$ excess between 0.2 and 0.25 keV. As an example, the boron spectrum of PG 1426+015 is shown in Figure 3. Since no other results of PSPC observations with the boron filter of bright sources have been published so far, we cannot ascertain the reality of this feature. However, its presence at about the same intensity in the spectra of quasars with very different energy slope would argue for its artificial origin. i.e., for rather large uncertainties in the knowledge of the transmission of the filter or in the combination filter-transmission resolution matrix. Therefore, in the following we consider the results from the boron filter data with caution.

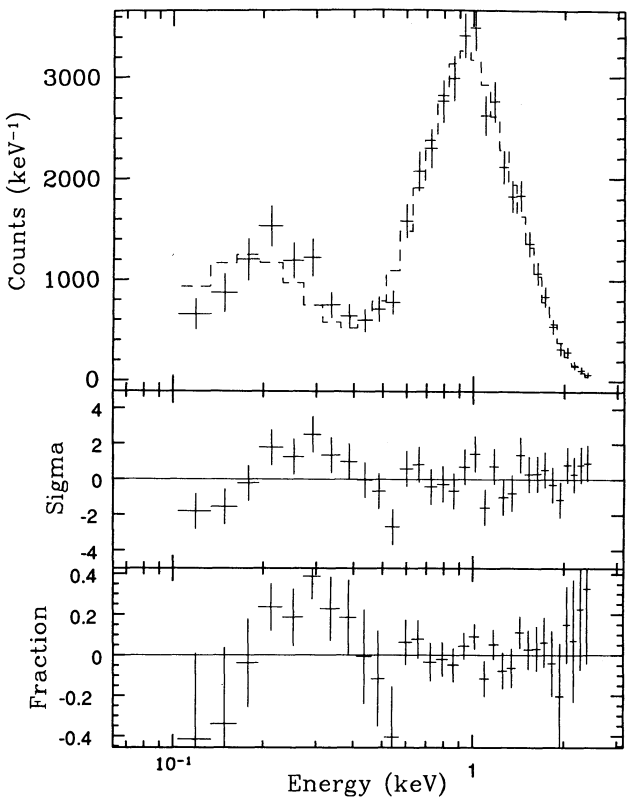

FIG. 3.—Single power law with low-energy absorption spectral fit to the boron filter spectrum of PG 1426+015.

3.2. *The Co-added Spectrum*

To test the reality of the deviations from the simple PL model suggested by the residuals in Figure 1, and to verify the existence of a break point between soft and hard spectra within the PSPC energy band, we added together the seven background-subtracted, 34 PI channel spectra of the five quasars observed with the open PSPC-B, to improve the signal-to-noise ratio. This procedure has been used several times before in X-ray astronomy (see, e.g., Pounds et al. 1990). The resulting spectrum contains about 50 kcounts (2130 counts above 1.5 keV), and its quality is similar to that of good PSPC spectra of nearby Seyfert galaxies. The signal-to-noise

TABLE 4

POWER-LAW SPECTRAL FITS TO THE BORON FILTER DATA

Name	Norm[a]	α_E	N_H^b	$\chi^2(dof)$	Prob. (%)
NAB0205+024	0.97 ± 0.05	2.22 ± 0.24	2.76 ± 0.44	25.72 (21)	21.7
PG1211+143	1.63 ± 0.11	1.95 ± 0.28	2.69 ± 0.55	23.85 (17)	12.3
MKN205-tot.	3.22 ± 0.15	1.25 ± 0.17	2.43 ± 0.46	28.49 (22)	16.0
PG1244+026	0.49 ± 0.06	2.23 ± 0.50	2.00 ± 0.85	15.37 (8)	5.3
PG1426+015	4.31 ± 0.14	1.50 ± 0.12	2.27 ± 0.22	43.97 (29)	4.8

[a] Flux density in units of 10^{-3} cm^{-2} s^{-1} keV^{-1} at 1 keV.
[b] In units of 10^{20} cm^{-2}.

ratio of ~200 is adequate to investigate the reality of the break point around 1 keV.

A concern with this approach is that spurious curvature in the co-added spectrum could be generated by adding together spectra with very different shapes. The Galactic N_H along the line of sight and the redshifts of the five quasars are similar, but the spread of α_E is wide, $\Delta\alpha_E \sim 1$. We therefore produced a simulated composite spectrum by simulating the observation of each quasar assuming a simple power law with the best-fit parameters in Table 3, and added together the resulting spectra. The χ_r^2 obtained by fitting the PL model to the simulated composite spectrum is close to 1 (see Table 3) and assures us that no spurious feature has been artificially introduced into the real composite spectrum. The best-fit α_E and N_H are in good agreement with the mean quasar slope and column density.

We then fitted the real co-added spectrum with the PL model. This produces spectral parameters very similar to those of the simulated spectrum but with an unacceptable χ_r^2 of 1.84 (for 29 degrees of freedom [dof] corresponding to a probability of 0.37%). The behavior of the residuals (Fig. 4*a*, *lower panels*) shows that the high χ^2 is not produced by random fluctuations but, rather, is due to a systematic wiggling, i.e., *an excess of counts between* 0.2 *and* 0.4 keV, *a deficit between* 0.6 *and* 1.5 keV, *and an excess above* 1.5 keV. To show quantitatively that this is the case, we binned up the 32 channel spectrum to obtain a 10 channel spectrum and fitted it again with the PL model. The χ_r^2 is now 4.016 (7 dof, corresponding to a probability of 0.040%). The residuals after subtracting the best-fit PL model from the binned composite spectrum are shown in Figure 4*b*. The wiggling is evident as the excess in the last three channels.

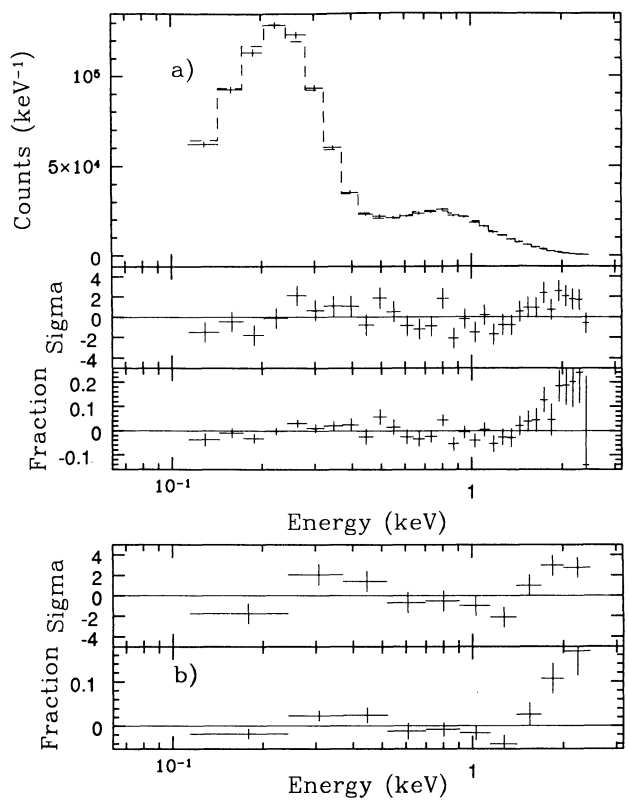

FIG. 4.—Single power law with low-energy absorption spectral fit to the composite spectrum obtained by adding together those of NAB 0205+024, PG 1211+143, MKN 205, TON 1542, and PG 1244+02. Energies are in the observed frame.

Excluding the last channel at 2–2.45 keV, where the amplitude of the systematic error can be high (~25% according to *ROSAT* Status Report #39, but see also Appendix A) does not ameliorate the χ^2 sufficiently ($\chi_r^2 = 3.46$, 6 dof, probability = 0.25%) or change the shape of the residuals. If the features are not real, they imply large systematic errors of 5% to 10% of the counts in each channel in the 0.1–2 keV PSPC band which are probably unreasonable (but might be due to an uncalibrated gain shift?) and of ~20% above 2 keV. Furthermore, the comparison between the PSPC and the 2–10 keV spectra of these quasars (see § 3.1) suggests a break between the soft and hard components at ~1 keV, and this break can account for the observed features (§ 3.4 below). We conclude that the features are likely to be present in the intrinsic source spectra.

The next step was to fit the data with more complex models. The PL model can be modified either in the absorption law or in the emission law used. We consider both modifications in the following.

3.3. *Complex Absorption*

The simple absorption model we considered in the previous section can be modified in several ways. We tried two possibilities, both of which have been suggested in the case of other AGNs: an inhomogeneous, neutral, partial covering absorber (PC model), and a uniform, ionized absorber (parameterized by an absorber of column density N_{H1} above an energy E_0 and another absorber of column density N_{H2} below E_0, i.e., by the inclusion of an absorption edge). Both models require the inclusion of two additional parameters. The PC model produces a significant improvement in χ^2 both in the composite spectrum (see Table 5) and in the individual spectra of four of the six quasars (NAB 0205+024, MKN 205, TON 1542, and PG 1426+015; see Table 6). The inclusion of one absorption edge produces a slight improvement in χ^2 in the composite spectrum with respect to the PL model, but an improvement in χ^2 for NAB 0205+024, MKN 205, and TON 1542 similar to that obtained using the PC model. The energy of the edges (quasar frame) in these three cases is in fact different: $0.97^{+0.15}_{-0.10}$ in NAB 0205+024; 0.61 ± 0.30 in MKN 205; and $0.29^{+0.26}_{-0.10}$ in TON 1542. Fitting a power law with two edges to the composite spectrum reduces the χ^2 to 25.4. The depth of the edges is much smaller than that in warm absorber sources such as MCG −6-30-15 (Nandra & Pounds 1992), 3C 351 (Fiore et al. 1993), NGC 3783 (Turner et al. 1993b), PG 1114+445 (Laor et al. 1994).

The best-fit slope in both the PC model and in the models including edges is always similar or even steeper than that obtained fitting the PL model and, again is inconsistent with the higher energy slopes of radio-quiet quasars. We therefore conclude that complex absorption *alone* cannot simultaneously explain the features in the fit with the PL model and the inconsistency between the present PSPC and higher energy measurements.

3.4. *Curved Single Emission Component Models*

The simplest modification to the single-component PL model, the one requiring just one additional parameter, is the assumption of a variable slope (e.g., Schwartz & Tucker 1988).

TABLE 5

SPECTRAL FITS TO THE COMPOSITE SPECTRUM

model	α_E	2nd Parameter	3rd Parameter	χ^2 (dof)	F
1 - P.L.[a]	1.69 ± 0.037			53.47 (29)	
2 - Partial Covering[b]	1.83 ± 0.28	$N_H = 2.4^{+2.7}_{-1.3}$	$C_f = 0.53 \pm 0.25$	25.97 (27)	28.6
2a - Variable. slope lin [c]	1.95 ± 0.11	$\beta = 0.27 \pm 0.10$		27.55 (28)	26.3
2b - Variable slope log [c]	1.65 ± 0.11	$\beta = 0.50 \pm 0.20$		31.15 (28)	20.1
3 - Broken P.L.[b]	$1.14^{+0.35}_{-0.64}$	$\alpha_S = 1.81^{+0.10}_{-0.08}$	$E_0^d = 1.24 \pm 0.29$	25.95 (27)	28.7
4 - 2 P.L.[b]	< 1.11	$\alpha_S = 1.91^{+0.54}_{-0.14}$	$R(1)\frac{H}{S}^e = 0.1^{+0.60}_{-0.07}$	26.81 (27)	26.84
4 - 2 P.L.[c]	1.0FIX	$\alpha_S = 2.34 \pm 0.25$	$R(1)\frac{H}{S}^e = 1.06 \pm 0.35$	30.90 (28)	22.8
4b - P.L.+ P.L.cutoff[b]	1.0FIX	$\alpha_S = 0.50 - 0.65$ $E_{cut} = 0.24 \pm 0.04$	$R(1)\frac{H}{S}^e = 4.6 \pm 1.4$	30.82 (27)	19.84
5 - P.L. + T. Bremss.[b]	$1.27^{+0.27}_{-0.45}$	$T = 0.19 \pm 0.06^d$	$R(1)\frac{P.L.}{T.B.}^e = 12.5^{+10}_{-5}$	29.12 (27)	22.6
5 - P.L. + T. Bremss.[c]	1.0FIX	$T = 0.23 \pm 0.02^d$	$R(1)\frac{P.L.}{T.B.}^e = 5.1 \pm 1.5$	31.45 (28)	19.6
6a- P.L. + Raym. A=0[b]	$1.27^{+0.27}_{-0.39}$	$T = 0.20 \pm 0.07^d$	$R(1)\frac{P.L.}{Raym.}^e = 11.5 \pm 5$	29.24 (27)	22.4
6b- P.L. + Raym. A=0.3[b]	1.53 ± 0.11	$T = 0.12 \pm 0.03^d$	$R(1)\frac{P.L.}{Raym.}^e = 510^{+580}_{-260}$	34.98 (27)	14.3
6c- P.L. + Raym.[b]	1.0FIX	$T = 0.24^{+0.01}_{-0.03}{}^d$ A=0+0.004	$R(1)\frac{P.L.}{Raym.}^e = 4.6 \pm 0.6$	31.81 (27)	18.4
6d- P.L. + 2 Raym.	1.0FIX	$T1 = 0.13^d$ A=1FIX	$R(1)\frac{P.L.}{Raym.}^e = 4$ $T2 = 0.73^d$	23.39 (26)	33.4
7 - P.L. + Black Body[b]	1.47 ± 0.16	$T = 0.074^{+0.011}_{-0.017}{}^d$	$R(1)\frac{P.L.}{B.B.}^e = 180 \pm 80$	33.12 (27)	16.6
7 - P.L. + Black Body[c]	1.0FIX	$T = 0.091 \pm 0.004^d$	$R(1)\frac{P.L.}{B.B.}^e = 17 \pm 2$	69.50 (28)	-

[a] Errors 68% confindence intervals for two interesting parameters.
[b] Errors 68% confidence intervals for four interesting parameters.
[c] Errors 68% confidence intervals for three interesting parameters.
[d] In keV.
[e] $R(1)$ = ratio between the flux at 1 keV in the hard-to-soft components.

We considered both a slope linearly variable with the energy,

$$F(E) = C_\gamma e^{-\sigma(E)N_H} E^{-(\alpha-\beta E)} ,$$

and a slope logarithmically variable with the energy,

$$F(E) = C_\gamma e^{-\sigma(E)N_H} E^{-[\alpha-\beta \log(E)]} .$$

These simple models produce a very good fit to the composite spectrum (see Table 5 and Fig. 5), and the improvement in χ^2 with respect to the PL model is significant at better than 99.998% (by using the F-test, $F = 26.3$ and $F = 20.1$ for the linear and logarithmic models, respectively). Fitting the variable slope models to the spectra of each individual quasar produces a sizeable improvement in χ^2 in three cases: NAB 0205+024, $F = 11.4$; MKN 205, $F = 5.0$; TON 1542, $F = 12.7$ ($F = 47.5$ when N_H is fixed to the Galactic value; see Table 6). Fitting the variable slope models to the spectrum of PG

TABLE 6

χ^2 FOR FITS TO THE PSPC QUASAR SPECTRA

model	NAB0205+024 χ^2(dof) $N_H - N^a_{HGal}$	PG1211+143 χ^2(dof) $N_H - N^a_{HGal}$	MKN205 χ^2(dof) $N_H - N^a_{HGal}$	TON1542 χ^2(dof) $N_H - N^a_{HGal}$	PG1244+026 χ^2(dof) $N_H - N^a_{HGal}$	PG1426+015 χ^2(dof) $N_H - N^a_{HGal}$	Soft-7 χ^2(dof)
Power law	34.7 (27) 4	39.7 (27) 4	31.4 (29) 5	30.4 (28) -5.6	22.8 (25) 10	34.7 (29) -1	53.5 (29)
Partial Covering	19.7 (25) 9	39.5 (25) 5	26.7 (27) 11	25.5 (26) 0	22.5 (23) 10	26.4 (27) 0	26.0 (27)
Variable slope lin.	24.2 (26) 11.5	39.0 (26) 7	26.5 (28) 10.3	20.9 (27) -2.2	22.8 (24) 10	33.4 (29) 1	27.6 (29)
Variable slope log.	27.8 (26) 14	37.5 (26) 8.4	25.6 (28) 14.6	21.3 (27) 0	22.0 (24) 7	34.7 (29) 1	31.2 (29)
Broken P.L.	18.9 (25) 8.8	38.6 (25) 5	27.5 (27) 14.4	22.4 (26) -4.3	22.8 (23) 10	27.9 (27) 0	25.9 (27)
2 P.L.	25.1 (25) 11.7	37.5 (25) 7.5	25.5 (27) 14.6	21.6 (26) 0	22.8 (23) 10	34.0 (27) 1.6	30.9 (27)
P.L.+P.L.cutoff[b]	18.5 (24) 0	39.0 (24) 0	24.3 (26) 8.1	26.8 (25) 0	22.8 (22) 0	34.7 (26) 0	28.8 (26)
P.L.+T.Bremss.	18.4 (25) 0	39.4 (25) 0	27.5 (27) 7	26.4 (26) 0	22.8 (23) 0	42.4 (27) 0	31.5 (27)

[a] In units of 10^{19} atoms cm^{-2}.
[b] The slope of the cutoff power law is constrained within the range -0.5–0.5. The slope of the hard power law is constrained within the range measured by other experiments above 2 keV or within the range 0.5–1.3 when no good high-energy measurements are available (NAB 0205+024; PG 1244+026).

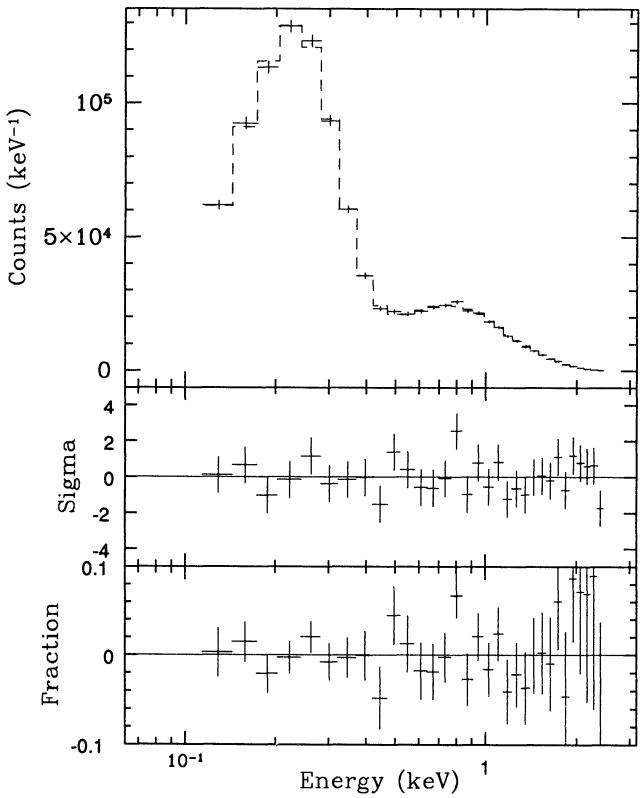

FIG. 5.—Variable spectral index model spectral fit to the composite spectrum. Energies are in the observed frame.

1426+015 does not produce a significant improvement in χ^2 ($F = 1$). Of course, the variable slope models are not physical models, since the spectral index diverges with the energy, rapidly toward the high energies in the linear model and both toward low and high energies, but less rapidly in the logarithmic model. They are only good parameterizations of the quasar spectra in the PSPC energy range. The linear model produces slightly better χ^2, and the logarithmic model produces slightly higher best-fit N_H (Tables 5 and 6).

The $\Delta\alpha_E$ between 0.2 and 2 keV found is 0.5 in the composite spectrum (0.8 in NAB 0205+024, 0.4 in MKN 205, 0.5 in TON 1542) compatible with the difference in average slope, fitting the PL model, between the PSPC and the higher energy spectra.

In the variable spectral index models the steepening between the flat 2–10 keV slope and the steep low-energy slope is gradual. To test a sharper break point we fitted a broken power-law model (model BPL) to the composite spectrum and to the single spectra of the six quasars. This model requires, however, two parameters in addition to those of the PL model, the break energy E_0 and the slope above E_0. The fit of the BPL model to the composite spectrum gives a χ^2_r of 0.96, $E_0 = 1.24 \pm 0.29$ keV, low-energy and high-energy slopes of 1.8 ± 0.1 and $1.1^{+0.4}_{-0.6}$, respectively. The latter slope, although not tightly constrained, is in agreement with the 2–10 keV slopes of radio-quiet quasars found by *EXOSAT* and *Ginga*. Fitting the BPL model to the spectra of the individual quasars produces an improvement in χ^2 with respect to the PL model similar to that obtained with the variable spectral index models in MKN 205 and TON 1542, and a significantly large improvement in χ^2 in NAB 0205+024 and PG 1426+015 (Table 6). The break energy in individual quasars is $E_0 = 1.4 \pm 0.3$ in NAB 0205+024, $E_0 = 1.3^{+0.5}_{-0.4}$ in MKN 205, $E_0 = 1.5 \pm 0.5$ in TON 1542, and $E_0 = 1.7 \pm 0.3$ in PG 1426+015 (quasar frame energies).

Excluding the channels above 2 keV does not change the $\Delta\chi^2$ between the PL model and the curved models in NAB 0205+024, MKN 205, and TON 1542 and does not change significantly the best-fit parameters, in particular, the break energy in the BPL model On the other hand, excluding the channels above 2 keV in PG 1426+015 produces a very good fit with the PL model, and the assumption of more complex models does not reduce significantly the χ^2. In fact, from inspection of Figure 1 it is clear that in this source the residuals after subtracting the PL model are large only above 2 keV. Because of the above-mentioned large uncertainties on the PSPC calibration above 2 keV, the detection of a break between the soft and hard component in this source is therefore uncertain.

We note that the two cases where the adoption of a curved model does not significantly reduce the χ^2 are those with the worst statistics: PG 1211+143 and PG 1244+026 with only 3800 and 5500 counts, respectively, between one-half and one-third of the counts in the spectra of the other quasars.

3.5. *Two-Component Models*

While an intrinsic curvature in the quasar 0.2–20 keV spectra is plausible, variability observations seem to suggest, at least in some objects, the existence of two separate continuum components dominating the spectrum above and below ~1 keV, respectively. This is the case in MKN 335, where the variations of the flux below 1 keV are not well correlated with those at higher energies (Turner & Pounds 1988). We therefore tried fits to our data with two-component models. The results of the fits to the composite spectrum are given in Table 5. The smallest χ^2 is obtained with the two power-law model (2PL). The χ^2 obtained with the power law + thermal bremsstrahlung model (PLTB) and the power law + Raymond-Smith (1977) thermal plasma model with zero metal abundance (PLRSa) are slightly higher ($\Delta\chi^2 = 2.3$, probability of 13%; $\Delta\chi^2 = 2.43$, probability of 12%), while that obtained with the power law + Raymond-Smith plasma with metal abundances fixed at the value $A = 0.3$ (PLRSb) and the power law + blackbody (PLBB) are significantly higher ($\Delta\chi^2 = 8.17$, probability of 0.4%, and $\Delta\chi^2 = 6.3$, probability of 1.2%, respectively). Fixing the high-energy spectral index to the value of 1, typical in radio-quiet quasars and close to that measured above 2 keV in all three of the five quasars making up the composite spectrum with *EXOSAT* or *Ginga* observations, produces acceptable fits with models 2PL and PLTB, a marginally acceptable fit with model PLRS ($\Delta\chi^2 = 5.0$, probability of 2.5%) and an unacceptable fit with model PLBB ($\Delta\chi^2 = 42.7$, probability $< 10^{-8}$). In the following, therefore, we will no longer discuss model PLBB.

Both the temperatures in the bremsstrahlung or Raymond-Smith parameterizations of the soft component and the slope of the soft power law in the power-law parameterization are reasonably well constrained to be $T \sim 0.2$ keV and $\alpha_E \sim 2$, respectively (see Table 5). The biggest difference among the results obtained with models 2PL, PLTB, and PLRS is the difference in the relative normalization at 1 keV between the hard and soft components, which is the order of 1 or less in the 2PL model, while it is higher than a few in the PLTB model.

For the PLRS model the χ^2 is smaller for metal abundances,

A, very close to zero. The main features introduced by a higher metal abundance in the PSPC band at the temperature of a few tenths of keV are strong O VII and O VIII lines at 0.57 and 0.65 keV and the iron L complex lines around 0.9 keV. The absence in the composite spectrum of any strong feature at those energies strongly constrains the metal abundance or for a given A, the relative strength of the thermal component. In fact, for $A = 0.3$ not only is the fit worse ($\Delta\chi^2 = 5.7$, probability of 1.6%), but the relative strength of the thermal component is reduced by a factor ~ 40 in comparison to the case with $A = 0$, its temperature is lower, and α_E is close to that obtained with the simple PL model. Fixing α_E at 1 puts a 99% upper limit on A of 0.01. The only way to obtain a good χ^2 fixing α_E at 1 and the metal abundance at 1 is to assume a two temperature model for the soft X-ray component ($T1 \approx 0.1$ keV, $T2 \approx 0.7$ keV). A similar situation applies to the case of several elliptical galaxies, where the PSPC data cannot discriminate between a low-metal-abundance single-temperature model and a solar-abundance two-temperature model (Trinchieri et al 1994).

We also fitted to the composite spectrum a power law + power law with exponential cutoff (PLPLCUT), fixing the high-energy spectral index to 1 and constraining the low-energy spectral index in the range -0.5–0.5, the typical UV slope of quasars. The fit is again acceptable, and the cutoff energy is 0.24 ± 0.04 keV, similar to the PLTB and PLRS temperature (but significantly different from the break energies used by Walter & Fink 1993 in a similar parameterization of PSPC spectra). In fact, the best-fit PLPLCUT model is practically indistinguishable from the best-fit optically thin thermal models (the slope of the soft power law is close to the bound of 0.5, which is similar to the asymptotic slope of a thermal bremsstrahlung spectrum).

3.6. *Two-Component Fits to the Spectra of Individual Quasars*

We repeated the fit with models 2PL, PLTB, PLRS, and PLPLCUT to the spectra of the six quasars, and the results are in Table 6. We constrained the spectral index of the harder power law to lie within the 90% confidence range found by *EXOSAT* and *Ginga*, when available, and between the 0.5 and 1.3, values typical in radio-quiet AGN, in other cases. As discussed by Saxton et al. (1993), possible changes in the high-energy spectral index between two different observations are probably smaller or close to the intervals in α_E considered here. We limited N_H to be greater than or equal to the Galactic value.

The PLRS model always gives a χ^2 higher than the PLTB model for $A < 0$. The PLRS model produces acceptable fits only for metal abundances close to zero in NAB 0205+024, $A < 0.01$, PG 1211+143, $A < 0.01$, MKN 205, $A < 0.02$, PG 1244+026, $A < 0.02$, and PG 1426+015, $A < 0.01$; ($1\ \sigma$ upper limits for four interesting parameters). The metal abundances is undetermined in TON 1542 because the best-fit temperature is less than 0.1 keV, so there are no strong emission lines above 0.2 keV in the total predicted spectrum. As in the case of the composite spectrum, in the single quasars the only way to obtain good χ^2 when the metal abundance is higher than 0.3 is to assume a two-temperature model for the soft X-ray component. Since the shape of the two-temperature solar-metal abundance Raymond-Smith spectrum is indistinguishable, for the PSPC, from the shape of single-temperature low–metal-abundance spectrum, and since the latter is similar to the bremsstrahlung spectrum, we no longer consider the Raymond-Smith models.

Again, in two cases (PG 1211+143 and PG 1244+026) the adoption of a complex two-component model does not improve the χ^2 with respect to the single PL model, as in the other four quasars. In MKN 205 models 2PL, PLTB, and PLPLCUT give similar χ^2 values. In NAB 0205+024 model PLTB and PLPLCUT are preferred ($\Delta\chi^2 = 6.7$) at the 99% confidence level, while in TON 1542 the 2PL model is preferred ($\Delta\chi^2 = 4.8$) at the 97% confidence level. In PG 1426+015 the PLTB model is not acceptable (probability of 0.3%), while the 2PL model is acceptable (probability of 17%). As noted in the Introduction, the inclusion of a Compton-reflected hard component (discovered in the spectrum of several low-redshift Seyfert galaxies) would steepen the slope of the primary component by $\Delta\alpha_E \approx 0.1$–0.3 to $\alpha_E \sim 1$. This is similar to the slope measured in three of the four quasars in this sample with high-energy data (the only exception being PG 1426+015). Allowing the spectral index of the intrinsic hard component of PG 1426+015 to be as steep as 0.9, thereby allowing for the existence of a robust Compton reflected component in this source, does not qualitatively change the result obtained with either models 2PL or PLTB. In particular the latter is still unacceptable at the 0.8% confidence level.

To calculate the confidence intervals for flux and luminosity of each component in a two component model (with free N_H) is not easy, since the parameters are all correlated with one another. For example, the anticorrelation between the normalizations of the two power laws and the correlation between the slope and the normalization of the soft power law are always very strong. This means that evaluating the confidence interval on the flux of each component assuming the extreme values of both normalizations and of both slopes overestimates them. To calculate accurate confidence intervals we therefore plotted for each spectrum the minimum χ^2 found at a grid of values for the parameters determining the flux, as a function of the flux and/or luminosity. We then evaluated the flux and/or luminosity confidence interval corresponding to $\chi^2_{\rm min} + 4.72$ ($1\ \sigma$ for four interesting parameters). As an example, in the case of NAB 0205+024 the 68% confidence intervals for four interesting parameters of the normalization and the slope of the soft component are $(4\text{–}10) \times 10^{-4}$ photons cm^{-2} s^{-1} keV^{-1} and 2.4–3.3, respectively. The 68% confidence interval of the 0.2–2 keV luminosity calculated using the above confidence intervals without taking into account the correlation between the parameters is $0.5\text{–}3.5 \times 10^{45}$ ergs s^{-1}, much broader than the actual confidence interval of $(1.5\text{–}2.8) \times 10^{45}$ ergs s^{-1}. This is because the data strongly exclude a very low normalization *together with a* very flat slope for the soft component.

The consequence of allowing N_H to be free to vary (for values greater than the Galactic value) is to introduce a large uncertainty on the source flux at the lower end of the energy band. Because of the very strong correlation between N_H and the normalization of the soft component, the flux in this component below 0.2 keV is practically undetermined. As an example, in NAB 0205+024 reducing the band from 0.1–2 keV to 0.2–2 keV reduces the relative error on the soft component luminosity from $\sim 100\%$ to $\sim 30\%$, and considering the luminosity at 0.4 keV instead of 0.2 keV reduces the relative error from $\sim 50\%$ to $\sim 25\%$. We therefore adopt the band 0.2–2 keV and the energy 0.4 keV for the following studies. Table 7 gives for each of the six quasars: the 0.2–2 keV total luminosity and that in the soft components only, the 0.4 keV and 1 keV soft component luminosity, the 2 keV total luminosity, and the relative normalization 1 keV (quasar frame) between soft and

TABLE 7

QUASAR LUMINOSITIES

name	Soft $L^a_{0.2-2}$	$\nu L^b_\nu(0.4keV)$	Component $\nu L^b_\nu(1keV)$	Total $L^a_{0.2-2}$	$\nu L^b_\nu(2keV)$	LogRatio(1keV)[c]
NAB0205+024 d -	$18.2^{+7.1}_{-4.2}$	$8.07^{+1.79}_{-2.09}$	$1.60^{+0.33}_{-0.63}$	$19.4^{+8.2}_{-4.0}$	$1.07^{+0.07}_{-0.12}$	$-0.50^{+0.60}_{-0.55}$
e -	9.8	$5.53^{+1.49}_{-0.60}$	$0.78^{+0.30}_{-0.30}$	12.6	$1.18^{+0.09}_{-0.09}$	
f -				14.1	0.89	
PG1211+143 d -	$5.2^{+3.1}_{-1.5}$	$2.46^{+0.90}_{-0.65}$	$0.74^{+0.33}_{-0.41}$	$5.8^{+3.9}_{-1.1}$	$0.56^{+0.10}_{-0.06}$	< 0.40
e -	2.52	$1.64^{+0.74}_{-0.25}$	$0.25^{+0.19}_{-0.10}$	4.8	$0.62^{+0.08}_{-0.07}$	
f -				5.19	0.53	
MKN205 tot. d -	$2.5^{+1.4}_{-0.7}$	$1.15^{+0.62}_{-0.20}$	$0.31^{+0.35}_{-0.10}$	$4.1^{+1.6}_{-0.9}$	$0.92^{+0.05}_{-0.04}$	$0.30^{+0.40}_{-1.4}$
e -	1.23	$0.77^{+0.34}_{-0.28}$	$0.124^{+0.16}_{-0.065}$	3.6	$0.94^{+0.06}_{-0.06}$	
f -				3.3	0.86	
TON1542 tot. d -	$1.8^{+1.0}_{-0.4}$	$0.71^{+0.43}_{-0.25}$	$0.135^{+0.225}_{-0.076}$	$2.9^{+0.6}_{-0.1}$	$0.44^{+0.02}_{-0.02}$	$1.0^{+0.4}_{-1.3}$
e -	0.91	$0.41^{+0.20}_{-0.07}$	$0.005^{+0.009}_{-0.003}$	2.9	$0.45^{+0.07}_{-0.07}$	
f -				2.42	0.39	
PG1244+026 d -	$1.4^{+0.4}_{-0.2}$	$0.72^{+0.12}_{-0.09}$	$0.22^{+0.013}_{-0.062}$	$1.4^{+0.4}_{-0.2}$	$0.088^{+0.012}_{-0.004}$	< 0.4
e -	0.79	$0.49^{+0.16}_{-0.04}$	$0.090^{+0.050}_{-0.032}$	1.0	$0.099^{+0.019}_{-0.015}$	
f -				1.41	0.090	
PG1426+015 d -	$6.0^{+1.2}_{-1.3}$	$3.21^{+0.49}_{-0.58}$	$1.69^{+0.29}_{-0.66}$	$7.0^{+1.2}_{-0.4}$	$1.43^{+0.12}_{-0.09}$	$-0.90^{+0.85}_{-0.15}$
e -	3.17	$2.22^{+0.54}_{-0.25}$	$0.144^{+0.115}_{-0.034}$	6.6	$1.56^{+0.14}_{-0.14}$	
f -				6.58	1.36	

[a] 0.2–2 keV luminosity in units of 10^{44} ergs s^{-1}.
[b] In units of 10^{44} ergs s^{-1}.
[c] Quasar frame.
[d] Two power-law model.
[e] Power law + thermal bremsstrahlung model.
[f] Single power-law model.

hard components, all calculated with models 2PL and PLTB. The errors represent the 68% confidence interval for four interesting parameters ($\Delta\chi^2 = 4.72$). As a comparison, Table 7 also gives the total 0.2–2 keV and 2 keV luminosities calculated with model PL.

3.7. *Comparison with IPC Observations*

We showed in § 3.1 that using a single power law with low-energy absorption model, the PSPC slopes are significantly steeper than the IPC slopes in three of the six quasars. In PG 1211+143 and TON 1542 the PSPC slopes are slightly steeper than the IPC ones but still compatible with them within the errors. In PG 1244+026 the IPC slope is poorly constrained, preventing a useful comparison with the PSPC result.

To investigate the difference between PSPC and IPC results we simulated the observation of quasars in the two instruments for a number of models and fitted the resulting spectra with the PL model. Assuming a single absorbed power law obviously does not produce any measurable difference in the PSPC and IPC best-fit slopes. The PSPC and the IPC slopes are also very similar (to within $\Delta\alpha_E \approx 0.1$) if the incident spectrum is formed by two summed power laws (with indices compatible with those found at high energy by *EXOSAT* and *Ginga* and at low energy by the PSPC). Only small differences were found for other two-component models, such as the PLTB and the PLRS models. The largest differences by $\Delta\alpha_E \approx 0.2$ in best-fit slopes occurred for models with a sharp break between the soft and hard component, such as the BPL model.

A quantitative comparison between PSPC and IPC spectra seems therefore capable of discriminating between different models for the soft X-ray emission of quasars. For this reason, we reextracted the IPC spectra of the six quasars from the "*Einstein* observatory database of IPC images in event list format" (Prestwich et al. 1992) and analyzed them together with the PSPC spectra. The IPC spectra of TON 1542 and PG 1244+026 contain only about 400 counts each, and therefore their inclusion in the fit does not change appreciably the results. The other four IPC spectra contain between 1000 and 7000 counts. In all fits the relative normalization between the two instruments is free to vary.

In the two-component models we required (1) the relative normalization between the soft and hard components to be the same in the two instruments, and (2) we let this normalization be free to vary independently in the two instruments. When fitting two component models or the BPL model, we limited the hard spectral index to the range observed by *EXOSAT* and *Ginga* or to the range 0.5–1.3 when no hard X-ray observation was available. We also limited the N_H to values greater than or equal to the Galactic one along the line of sight. The best-fit χ^2 obtained fitting models PL, BPL, and 2PL are in Table 8, along with the ratio between the normalizations at 1 keV in the two instruments (PSPC/IPC) for the PL model and the ratio between hard and soft components at 1 keV in the two instruments for the two-component models. In the case of NAB 0205+024 we report also the results obtained fitting the PLTB model since this model gives the best χ^2 in this source.

The flux at 1 keV is similar in the two instruments in the cases of MKN 205 and PG 1244+026, is marginally higher in the PSPC (~30%) in the cases of NAB 0205+024 and PG 1426+015, and is significantly higher in the PSPC in TON 1542 (a factor 2) and in the IPC in PG 1211+143 (a factor 3).

For two sources, PG 1211+143 and PG 1244+026, the fit with a simple power law is acceptable (or is not significantly worse than the fit with more complicated models). The ratio between the hard and soft component is therefore not well determined.

TABLE 8

χ^2 FROM SIMULTANEOUS FITS TO THE PSPC AND IPC DATA

model	NAB0205+024 χ^2 (dof)	PG1211+143 χ^2 (dof)	MKN205 χ^2 (dof)	TON1542 χ^2 (dof)	PG1244+026 χ^2 (dof)	PG1426+015 χ^2 (dof)
Power law	73.4 (35)	55.7 (35)	93.3 (38)	52.1 (37)	31.9 (32)	63.4 (36)
PSPC/IPC 1 keV	1.3	0.3	0.9	2.0	1.0	1.4
Broken Power law	35.4 (33)	55.7 (33)	63.1 (36)	45.4 (35)	30.92 (30)	40.08 (34)
2 power laws[a]	47.2 (33) 35[c]	55.7 (33)	67.4 (36)	40.7 (34)	32.4 (30)	53.7 (34)
[d]	0.5 (1.7[c])	0.	3.7	2.2	0.	0.3
2 power laws[b]	30.4 (32) 25.3[c]	50.3 (32)	36.4 (35)	25.3 (34)	29.53 (29)	36.9 (33)
[d]	0.4 0.9 (1.9 3.3)[c]	< 0.9 < 0.5	1.9 4.3	1.9 10.7	< 0.3 < 0.3	0.2 0.6

[a] The ratio between the two components is fixed in the two instruments.
[b] The ratio between the two components is free to vary in the two instruments.
[c] Power law + thermal bremsstrahlung model.
[d] Relative normalization of the two components (hard/soft) in the two instruments (PSPC/IPC).

For the other four sources, the fit with the two-component models is always significantly better when the relative contribution of the two soft and hard components are free to vary in the two instruments. However, in these models the IPC spectra require in all cases a harder spectrum, i.e., the ratio between the normalization at 1 keV of the hard to the soft component is always higher in the IPC. To understand this in terms of the model requires all the sources to have been in a much softer state (regardless of the overall intensity) during the PSPC observations. This seems unlikely, and, moreover, Figure 2*b* shows that the difference in slope between PSPC and IPC spectra is not confined to a few sources but, rather, that it is a systematic feature of the whole sample. Our conclusions, based on the above discussion and on the results presented in Appendix B, are that either (1) quasar spectra are much more complex than the parameterization adopted, or (2) there are large (10% to 20%) systematic uncertainties in the IPC calibration, probably around the oxygen edge at 0.54 keV, in the sense of an overestimate of the predicted counts at those energies, or (3) there are large (10% to 20%) systematic uncertainties in the PSPC calibration, probably in the knowledge of the efficiency of the instrument above 1 keV, in the sense of an overestimate of the predicted counts at those energies. Of course, any reasonable mix of the above hypotheses can also explain the discrepancy between PSPC and IPC measurements, requiring smaller (and maybe more reasonable) spectral complexity and calibration inaccuracies.

A major effort to verify the relative IPC and PSPC calibrations seems therefore unavoidable, in order to make full use of the high signal-to-noise PSPC-IPC spectra.

3.8. *Notes on Individual Objects*

1. *NAB 0205+024.*—The results of the spectral fitting suggest a sharp break between soft and hard components, such as that in the BPL model (where an intrinsic N_H is required at the 95% confidence level) or that in models in which the soft component is exponentially decreasing (PLTB and PLPLCUT, where, however, no additional N_H in addition to the Galactic one is required). Assuming no intrinsic absorption favors curved soft-component models, a soft component steep at high energy ($\gtrsim 1$ keV) and rather flat at low energy ($\alpha_S \sim 0.5$ at $E \lesssim 0.2$ keV).

Masnou et al (1992) detected a soft excess in this source analyzing an IPC/MPC observation performed on 1979 July. Because of the uncertainty in the relative calibration of IPC and PSPC, it is not possible to quantitatively compare the Masnou et al. (1992) results about the strength of the soft component with those presented in the above sections.

2. *PG 1211+143.*—The quasar was observed by the PSPC in a faint state, with a 1 keV flux corrected for Galactic absorption of $\sim 2 \times 10^{-3}$ keV cm^{-2} s^{-1} keV^{-1} (or 1.3 μJy), similar to the minimum of $\sim 1.7 \times 10^{-3}$ keV cm^{-2} s^{-1} keV^{-1} (1.1 μJy) detected during the 1986/008 *EXOSAT* observation, and about 3 times less than the maximum observed during the 1980/346 IPC observation (Elvis et al. 1991). Spectral variability has been detected by Elvis et al. (1991) in the sense that the source softens when it brightens. However, even at the minimum level recorded during 1991 December the PSPC spectrum is still completely dominated by the soft component. A detailed discussion of the PG 1211+143 *Einstein* and *EXOSAT* observations is given by Elvis et al. (1991). Saxton et al. (1993) analyzed three *EXOSAT* ME/LE observations parameterizing the spectrum with a PLTB model with N_H fixed at the Galactic value and a temperature of 0.2 keV for the thermal component. For the observation with the smallest source intensity (1986/008), they found a 0.1–2 keV total flux of 30×10^{-12} ergs s^{-1} cm^{-2} and a 0.1–2 keV flux of the thermal component of 16×10^{-12} ergs s^{-1} cm^{-2} (30% statistical error). Using the same model, we find a total 0.1–2 keV flux of 22×10^{-12} ergs s^{-1} cm^{-2} and a thermal component 0.1–2 keV flux of 12×10^{-12} ergs s^{-1} cm^{-2}. The PSPC fluxes are slightly smaller than the *EXOSAT* 1986/008 ones, but the ratio between the soft component flux to the total is still consistent with that found by Saxton et al. (1993).

3. *MKN 205.*—No significant spectral variability is detected between the two *ROSAT* observations presented in this paper, while the intensity changed by $\sim 25\%$. Small intensity variations and no large spectral variations are present in two *EXOSAT* LE/ME observations performed in 1983 November and 1984 January (LE and ME count rates were extracted from the HEASARC database).

Masnou et al. (1992) detected a soft excess analyzing an IPC/MPC observation performed in 1980 April. No strong soft excess was, however, detected in this source by Saxton et al. (1993) by using the two *EXOSAT* observations and the 2–10 keV slope measured by *Ginga*. Saxton et al. (1993) evaluated at $< 7.2 \times 10^{-12}$ ergs s^{-1} cm^{-2} (90 confidence) the 0.1–2 keV flux in any thermal component, and at $(13–16) \times 10^{-12}$ ergs s^{-1} cm^{-2} the total 0.1–2 keV flux (20% statistical error) in the two observations. The fit to the PSPC data with fixed N_H and fixed thermal bremsstrahlung temperature of 0.2 keV is highly unacceptable, and the 0.1–2 keV thermal component

flux is 3×10^{-12} ergs s^{-1} cm^{-2}. Allowing the temperature to be free to vary produces an acceptable fit ($\chi^2 = 31.6$, 28 dof), $T = 0.37 \pm 0.05$, a 0.1–2 keV thermal component flux of 7×10^{-12} ergs s^{-1} cm^{-2}, and a 0.1–2 keV total flux 18×10^{-12} ergs s^{-1} cm^{-2}. Letting N_H vary also reduces the χ^2 to 24.6 (27 dof) and gives $T = 0.22^{+0.11}_{-0.06}$, a 0.1–2 keV thermal component flux of 8.5×10^{-12} ergs s^{-1} cm^{-2}, and a 0.1–2 keV total flux of 23×10^{-12} ergs s^{-1} cm^{-2}. It is therefore not surprising that Saxton et al. (1993) did not detect the soft excess, since small changes in the value of the parameter N_H can substantially change the derived 0.1–2 keV flux in the soft component.

MKN 205 is the quasar in our sample with the strongest evidence of absorption in excess to the Galactic column. It is the only one with evidence of excess absorption even in the PLTB and PLPLCUT models. The N_H obtained by fitting the 2PL model is $4.2 \pm 0.8 \times 10^{20}$ atoms cm^{-2} (1 σ error for four interesting parameters), and the difference in χ^2 obtained fixing N_H to the Galactic value of 2.74×10^{20} atoms cm^{-2} (Elvis et al. 1989) is $\Delta\chi^2 = 29.0$, significant at better than 99.9999% confidence. The N_H obtained by fitting the PLTB model is $3.5 \pm 0.6 \times 10^{20}$ atoms cm^{-2}. Fixing N_H to the Galactic value gives a $\Delta\chi^2$ of 7, significant at the 90% confidence level.

Excess absorption similar to that due to our galaxy in this source is not surprising, since its projected position on the sky lies within the spiral arms of the nearby, face-on galaxy NGC 4319 (at a redshift of 0.00468; see Sulentic & Arp 1987). Two resonant absorption lines, the Mg II doublet, produced by the gas in the intervening galaxy have been recently detected by Bahcall et al. (1992).

4. *TON 1542.*—A soft excess in this source has been detected by Comastri et al. (1992) analyzing the *EXOSAT* ME/LE observation of 1985 May.

Contrary to our results for NAB 0205+024, the assumption of no intrinsic absorption here favors a steep power-law soft component. Alternatively, modeling the soft component as a thermal bremsstrahlung or as a power law with exponential cutoff and flat low-energy spectral index suggests the existence of an additional ultrasoft component.

5. *PG 1244+026.*—This source was observed by the open PSPC on 1991 December 22 and 24 and by the PSPC covered with the boron filter on 1991 December 24. The source intensity between the two days dropped by a factor of 2 (as is also clear comparing the count rates in Tables 1 and 2) without any large variation of the spectral shape. As in the case of PG 1211+143, the PSPC spectrum of PG 1244+026 is completely dominated by the soft component.

6. *PG 1426+015.*—Masnou et al. (1992) do not find evidence for a large soft excess in this source in two IPC/MPC observations performed on 1980 August and 1981 January. However, a soft excess has been reported in this source by Comastri et al. (1992) analyzing an *EXOSAT* ME/LE observation performed on 1985 June. (Some spectral resolution below 2 keV was achieved in this occasion by using all the three filters available for the LE: 3 Lexan, Al/pa and boron.) While the mean *EXOSAT* ME/LE slope (fixing N_H to the Galactic value) was consistent with the IPC/MPC one, the hard ME (2–10 keV) slope was significantly flatter than that reported by Masnou et al. (1992), giving rise to a strong soft excess in the LE. A soft excess has also been reported in the same *EXOSAT* observation by Saxton et al. (1993). We confirm the presence of a strong soft excess in this source. Saxton et al. (1993), parameterizing the spectrum with a PLTB model (which we find unacceptable, or marginally acceptable assuming a strong contamination of the 2–10 keV spectrum by an additional flat reprocessed component), evaluated the 0.1–2 keV flux of the thermal component at 17.9×10^{-12} ergs s^{-1} cm^{-2} and the total 0.1–2 keV flux at 23.8×10^{-12} ergs s^{-1} cm^{-2} (both with a 20% statistical error). By using the same model, we find $T = 0.24 \pm 0.03$, a 0.1–2 keV thermal component flux of 20×10^{-12} ergs s^{-1} cm^{-2}, fixing the hard slope at the *EXOSAT* value of 0.46, or 15×10^{-12} ergs s^{-1} cm^{-2} for our best-fit hard slope 0.9 (the upper limit of the available range), and a 0.1–2 keV total flux 28×10^{-12} ergs s^{-1} cm^{-2}, both fluxes being consistent with the above *EXOSAT* values.

4. DISCUSSION

4.1. *The Shape of the Soft X-Ray Spectrum*

The high quality PSPC spectra of six quasars are all roughly consistent with a single absorbed power-law model. The deviations from this model are smaller than 20% at all energies. This simple parameterization yields slopes much steeper (by $\Delta\alpha_E \approx 0.5$–1) than those measured at higher (2–10 keV) energies, a difference definitely larger than the systematic error on PSPC slopes estimated in Appendix A. A similar result was also obtained by several other authors (e.g., Turner, George, & Mushotzky 1993a; Walter & Fink 1993; Laor et al. 1994). These findings suggest that the PSPC spectra are dominated by a single *broad* soft component.

Although the deviations from a simple power law are small, the high signal-to-noise ratio of the PSPC observations allowed us to detect in the composite spectrum a significant excess above 1.5 keV, associated with a deficit of counts between 0.6 keV and 1 keV, with respect to the PL model. Similar features are present in the single spectra of NAB 0205+024, MKN 205, TON 1542, and PG 1426+015. Fitting more complex models significantly improves the χ^2 both in the composite spectrum and in these four cases.

A modification of the absorption law alone cannot explain both the features found in the PSPC spectra and the difference between the PSPC slope and the 2–10 keV one. This can be done by modifying the emission law. The PSPC spectra can statistically discriminate between many of the different curved or multicomponent models that can be reasonably associated with the soft X-ray spectrum of quasars: a blackbody, or a line, plus PL model cannot give a good fit to the data if the power-law slope is fixed at the typical value measured above 2 keV; a Raymond-Smith model can give a good fit only for either very small metal abundances or two temperatures. The results obtained for the two curved single-component models suggest that quasar spectra do not continue to steepen toward low energies, since the fits with the logarithmic model, where the slope at low energy continues to steepen, are always comparable to or worse than those with the linear model, where the slope at low energy quickly saturates at a constant value.

The PSPC data of PG 1211+143 and PG 1244+026 are well fitted by a single PL model, and no improvement in χ^2 is obtained by fitting more complex models. This is likely to be due to the fact that these two sources have the worst signal-to-noise ratio in the present sample and/or to a relatively small contribution by a hard component in the PSPC band. A sharp break between soft and hard components like that in the broken PL model is suggested in PG 1426+015. Using the additional constraint of assuming no intrinsic absorption favors curved soft-component models (flatter at low energy

and steeper at high energy) in NAB 0205+024, PG 1211+143, MKN 205, and PG 1244+026 and a steep power-law soft-component in TON 1542. All the above suggest that the diversity of soft X-ray spectra of quasars, pointed out first by Elvis, Wilkes, & Tananbaum (1985), is probably not due only to a different overall soft X-ray slope, but also to a different shape of the soft component or components.

We do not find in our analysis any evidence for narrow emission features. This does not mean that we can put strong limits on line emission in these quasars, since the PSPC energy resolution does not permit us to disentangle simple continuum models with no (or weak) lines from complex continuum models with multiple strong lines. We can, however, put strong limits on physical models containing a fixed mix of continua and lines, as for the case of an optically thin thermal emission from an ionized plasma. In this case we found very tight limits on line emission (mainly the oxygen Kα and iron L emission lines) and therefore on the metallicity of the gas. We therefore conclude that models of soft X-ray emission from a single-temperature ionized plasma are unlikely in these quasars unless the physical conditions are such that the continuum is optically thin while the strong soft X-ray lines are optically thick.

Ross & Fabian (1993) calculated the reflection spectrum from a slab of gas at $R = 7R_S$ under the assumption that the illuminating hard flux equals the soft flux locally produced in the slab. They found that the ionization parameter of the gas is proportional to the accretion rate and determines the emerging spectrum. Ross & Fabian (1993) give the 0.3–2 keV and the 2–20 keV spectral indices obtained from a least-squares fit of a power-law continuum to their total spectrum. The $\Delta\alpha_E$ between the low-energy and high-energy slope is of the order of 0.4, independent of the ionization parameter (and therefore from $L/L_{\rm Edd}$). This is similar to the $\Delta\alpha_E$ found between the soft and high-energy slopes of the four quasars in this sample with high-energy measurements, and to the $\Delta\alpha_E$ between the mean PSPC slope in Walter & Fink (1993) and the *Ginga* slope in Williams et al. (1992). For low accretion rates (corresponding to $L/L_{\rm Edd} = 0.15$), and low ionization parameters, the total emitted soft X-ray spectrum is rich, dominated by strong O VIII Kα and Fe XVII and XVIII Lα lines. For higher accretion rates ($L/L_{\rm Edd} = 0.30$), the strength of the line features is much reduced. The limits on the emission-line strength found in the previous sections argue for high accretion rates.

The photoionized gas can imprint sharp "jumps" on the emitted spectrum, since the gas opacity can suddenly change in the proximity of the many strong absorption edges present in the soft X-ray band. This is intriguing, since at least in some cases our fits to the PSPC spectra prefer a sharp break between the soft and hard components.

4.2. *Absorption Along the Line of Sight*

Most previous quasar studies found low-energy absorption consistent with (or even lower than) the Galactic one along the line of sight when fitting the data with a single PL model (e.g., Wilkes & Elvis 1987). The only exceptions are high-redshift radio-loud quasars (Elvis et al. 1994b), "warm absorber" sources (Pan, Stewart, & Pounds 1990, Nandra & Pounds 1992; Fiore et al. 1993; Turner et al. 1993c; Laor et al. 1994), and a few other intermediate-redshift radio-loud quasars (Marscher 1988; Allen & Fabian 1992; Elvis et al. 1994a).

The present analysis put an upper limit of $\sim 10^{20}$ atoms cm^{-2} on the $N_{\rm H}$ in addition to the Galactic one in all the quasars analyzed. The best-fit $N_{\rm H}$ is different in the different models adopted to fit the data. This means that assuming a particular value for $N_{\rm H}$ would discriminate between different models. In particular, a low $N_{\rm H}$, close to the Galactic one, favors curved soft component models as noted in the previous section. Unfortunately, the actual value of the best-fit $N_{\rm H}$ depends also on the accuracy of the calibrations at the low-energy end of the PSPC band. In Appendix A we show that there is a systematic positive difference of about 5×10^{19} between the $N_{\rm H}$ obtained with the 1993 January and 1992 March resolution matrices, the "1992 March" derived $N_{\rm H}$ values being generally in better agreement with the Galactic ones. A best-fit value of $N_{\rm HGal} + 5 \times 10^{19}$ could therefore still be within the calibration systematic uncertainties.

It is nevertheless worth noting that the only case among the quasars in our sample in which we have some rather model-independent evidence of $N_{\rm H}$ larger than the Galactic one (MKN 205) is the one in which an excess is reasonably expected, since the line of sight to this quasar intercepts the nearby galaxy NGC 4319.

5. SUMMARY

We have presented high signal-to-noise ratio, soft X-ray (0.1–2.5 keV) spectra of six radio-quiet, low-redshift, quasars. We summarize our main results and conclusions in the following.

1. The PSPC spectra span a broad range of slopes ($1.3 < \alpha_E < 2.3$) and are steeper than at high energies by $\Delta\alpha_E = 0.5$–1. They are dominated by the so called soft X-ray excess (above the extrapolation of the higher energy power law).

2. The deviations from a single PL model are small but still significant. The "break point" between the hard and soft components is typically in the "keV" region, at energies somewhat higher than those suggested in previous investigations. The PSPC spectra exclude "narrow" models, such as a line or a blackbody, for the soft X-ray component.

3. The modeling of the PSPC spectra suggests that the diversity of soft X-ray spectra of quasars is probably due not only to a different overall soft X-ray slope, but also to different shapes of the soft component or components. To confirm or reject this point, soft X-ray observations with instruments with better energy resolution than the PSPC, such as those on board *Asuka*, are needed.

4. The strength of any line emission feature in the soft X-ray band is small (less than 10%–20% of the counts in each channel), unless the continuum is very complicated. This is puzzling, since many different models predict the existence of such lines: "warm absorbers" (Netzer 1993; but see also Fiore et al. 1993, 1994), reprocessing from a disk (Ross & Fabian 1993), and optically thin ionized plasmas with temperatures between 0.1 keV and 1 keV. In the latter case, the absence of strong line features argue against emission from an ionized plasma as the main contributor to the soft X-ray component, unless there is a distribution of temperatures (at minimum a $T \sim 0.1$ and a $T \sim 0.7$ keV plasmas). More generally, this could suggest peculiar physical conditions for the soft X-ray emission region and the nearby regions that is, either high temperatures and ionization states (high $L/L_{\rm Edd}$ in the models of Ross & Fabian 1993) or a nonthermal origin for the soft X-ray emission.

5. No absorbing column density above the Galactic one is necessary in any of the quasar spectra greater than $\sim 1 \times 10^{20}$

atoms cm^{-2}. The only case in which an excess is suggested is MKN 205, where the line of sight intersects the galaxy NGC 4319.

6. Finally, we quantitatively compared PSPC and IPC spectra of the quasars in this sample and of other strong X-ray sources, finding a significant discrepancy. This suggests that, in principle, the combined analysis of the data in the two instruments can allow one to discriminate between model spectra better than the analysis of the data in one single instrument. The discrepancy, however, could be due to some inaccuracy in the calibration of one (or both) instruments. We conclude, therefore, that to make full use of the high signal-to-noise ratio PSPC-IPC spectra, a major effort to study and possibly revise the relative PSPC-IPC calibration is needed.

We thank Jeff Orszak for help in the data reduction and Stuart Daines, Jane Turner, Ian George, Rick Harnden, Larry David, Jack Hughes, and Paul Gorenstein for useful discussions on the PSPC and IPC calibration. We thank Jack Hughes for allowing us to use his PSPC N132D data. This research has made use of data obtained through the High Energy Astrophysics Science Archive Research Center Online Service, provided by the NASA/Goddard Space Flight Center, and through the Einstein On-Line Service, Smithsonian Astrophysical Observatory. This work was supported by NASA grants NAGW-2201 (LTSARP), NAG 5-1872, NAG 5-1883 and NAG 5-1536 (*ROSAT*), and NASA contracts NAS 5-30934 (RSSDC), NAS 5-30751 (*HEAO 2*) and NAS 8-39073 (ASC).

APPENDIX A

PSPC RESPONSE MATRICES

We present here a comparison of the two "official" response matrices, those released on 1992 March 12 and on 1993 January 11, and a discussion of the amplitude of the residual systematic uncertainty in the 1993 January matrix at energies higher than 0.5 keV.

Three strong systematic features (5% to 10% of the counts in each channel) were found in the residuals of PSPC spectral fits with the official response matrix released on 1992 March (DRM_9): a deficiency of measured counts above the carbon edge (0.3–0.5 keV) with the associated excess around 0.2 keV, an excess between 0.7 and 0.9 keV, and an excess above 2 keV. These features have been corrected in the new resolution matrix (DRM_36_1) released in 1993 January, which was obtained by "fudging" the response matrix values with the residuals after subtracting the best-fit broken power law with Galactic absorption model from the spectrum of the bright BL Lacertae object MKN 421 observed with the PSPC in 1992 May (Hasinger & Snowden 1992). In many cases the fits with the 1993 January matrix give a better χ^2 than those with the 1992 March matrix, but for a number of sources the opposite is true. This is shown in Figure 6, where we report the χ^2_r obtained with both matrices fitting a simple power law with low-energy absorption model to the spectra of 26 AGNs with more than 1000 counts each. Filled symbols identify observations of the quasars presented in this paper. Squares identify observations performed before 1991 October 14 with a high-gain setting, and circles identify the observations performed after 1991 October 14. Most of the quasars with a χ^2 higher with the 1993 January matrix than with the 1992 March matrix were observed with the high-gain setting. In particular, a large deficit in the observed counts with respect to the best fitting PL model is observed in these spectra between 0.1 and 0.2 keV when they are fitted with the 1993 January matrix. A time variation of the PSPC gain which is not included in the correction process currently applied to data in SASS has been recently confirmed by two other independent analyses performed at MPE and NASA/GSFC (*ROSAT* Status Report #64).

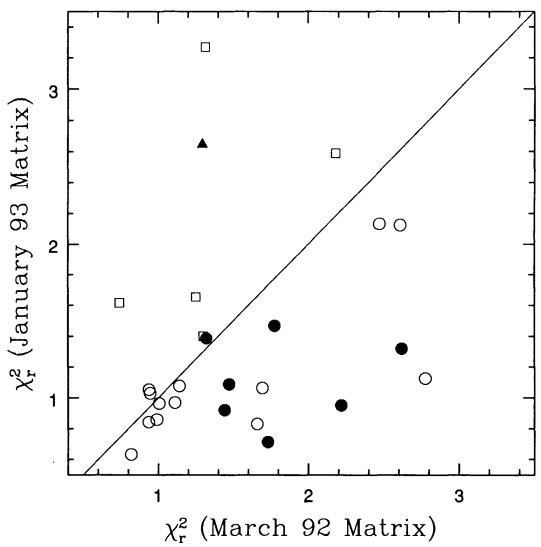

FIG. 6.—Reduced χ^2 obtained by fitting a simple power law with low-energy neutral and uniform absorption to the spectra of 26 AGN (with more than 1000 counts each), employing the resolution matrices released on 1992 March and 1993 January. Circles identify observations performed with PSPC B after 1991 October (i.e., with the low-gain setting), while squares identify observations performed before 1991 October (i.e., with the high gain setting). (*Triangle* identifies an observation performed with PSPC A during the PV phase.) Filled symbols identify quasar observations reported in this paper. All observations which give a significantly higher χ^2 value with the 1993 January matrix than with the 1992 March matrix were acquired with the high-gain setting (or with PSPC A).

We therefore conclude that the 1993 January matrix should be use for observations after 1991 October, while the 1992 March matrix is preferable for observations before 1991 October. Only one of the quasars in our sample was observed before 1991 October (PG 1426+015, observed with the PSPC-A), and we will therefore use the 1992 March matrix only for this source. The other quasars were observed between 1991 November and 1992 July in all cases within 6 months from the MKN 421 observation.

The number of counts predicted in the 0.1–0.3 band by using the 1993 January matrix is systematically larger than that predicted with the 1992 March matrix, probably because the overall efficiency at those energies has been increased by 20% at 0.1 keV, 5% at 0.2 keV, and 2.5% at 0.28 keV. This results in an increase of $\sim 5 \times 10^{19}$ atoms cm^{-2} in the best-fit N_H and an increase of ~ 0.2 in the best-fit α_E, in the fits with the 1993 January matrix, with respect to the fits with the 1992 March matrix. This is shown in Figures 7*a* and 7*b*, where the plot for the same sample of AGNs the N_H and the α_E obtained with both matrices. Column densities obtained with the 1992 March matrix agree with the Galactic column densities in the direction of the quasars generally better than those obtained with the 1993 January matrix, as is shown in Figures 8*a* and 8*b*.

The 1993 January matrix was calibrated using an observation performed in 1992 May in the low-gain setting, while the 1992 March matrix was calibrated using observations performed at the beginning of 1991 in the high-gain setting. Thus, they should be appropriate, at least with regard to the best-fit parameters, to observations performed around these two periods. Observations performed in-between could have gains slightly different from those in the observations used to calibrate the matrices, and therefore fitting them with one of the two matrices would produce a small systematic error in the best-fit parameters. We evaluate the maximum amplitude of this systematic error as the difference in the best-fit parameters obtained using both matrices, i.e., $\sim 5 \times 10^{19}$ atoms cm^{-2} on N_H and ~ 0.2 on α_E (see also Turner 1993). We note that the best-fit N_H and α_E in the two observations of MKN 205 and TON 1542 performed on 1991 November and 1992 April and on 1991 December and 1992 July, respectively, are within the above uncertainties (see Table 3).

Above ~ 0.3–0.4 keV the fits with the 1993 January matrix are always better than those with the 1992 March matrix and are apparently free from strong systematic features. It is, however, important to quantify the magnitude of any possible "narrow" systematic feature. For this purpose, we cannot use AGN spectra, since they show a complex curved continuum in this energy band, with, possibly, edges and lines superposed. Possible calibration candidates are hot and bright clusters of galaxies not highly obscured by Galactic absorption. We chose an observation of the central region of the Coma Cluster, one of the brightest and best studied clusters of galaxies in the X-ray band. We extracted from the *ROSAT* archive the observation performed on 1991 June 18

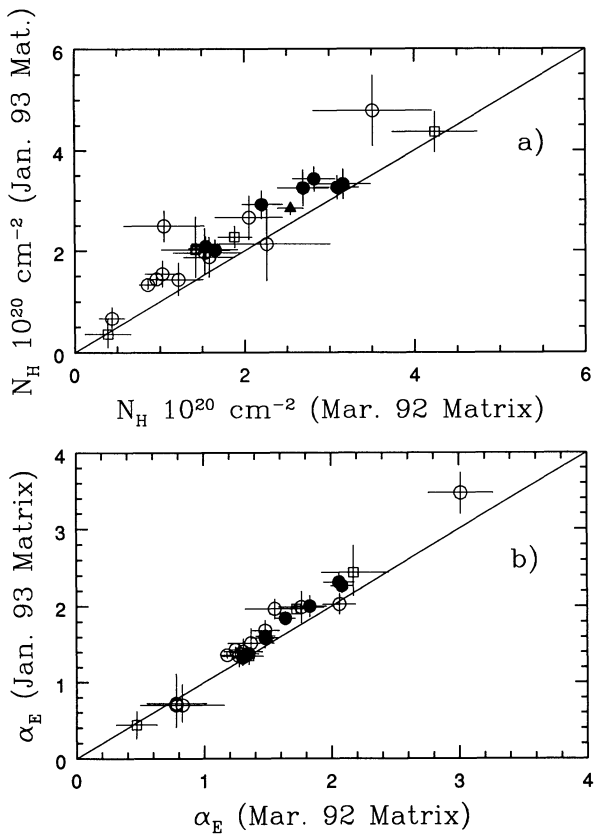

FIG. 7

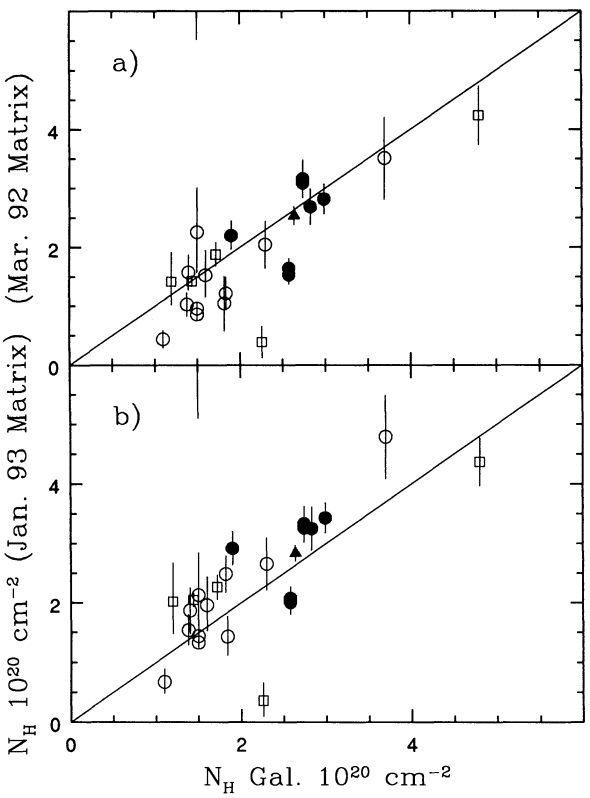

FIG. 8

FIG. 7.—The N_H and the α_E obtained for the same sample as Fig. 6 with both matrices. Symbols are the same as in Fig. 6.

FIG. 8.—The N_H obtained for the same sample as Fig. 6 with both matrices plotted as a function of the Galactic N_H along the line of sight. Symbols are the same as in Fig. 6. Column densities obtained with the 1992 March matrix agree with the Galactic column densities in the direction of the quasars generally better than those obtained with the 1993 January matrix.

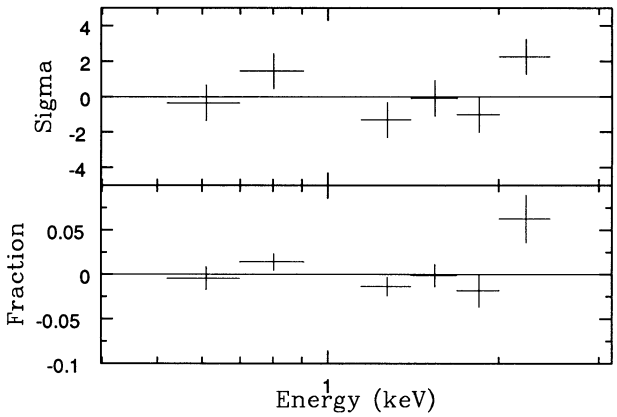

FIG. 9.—The residuals after the subtraction of the best-fit Raymond-Smith model from the Coma spectrum for the fit with the 1993 January matrix both as number of σ and as a fraction of the counts in each channel. The spectrum has been rebinned to enhance any systematic deviation. No strong systematic feature is present in the residuals from the fit.

(by principal investigator S. White). Unfortunately, this observation was performed with the high-gain setting and thus probably produces a bad fit below 0.5 keV when fitted with the 1993 January matrix.

The core of the Coma Cluster was observed for 20,220 s. We extracted a spectrum from an on-axis circle of radius 5′. We collected about 83,500 counts in the 0.1–2.45 keV energy band (49,200 in the 0.5–2.45 keV band). We tried three different background subtractions: (1) we estimated the background from a region 30′ off-axis and corrected it for the energy-dependent vignetting (note that at this off-axis angle the emission from the cluster itself is still rather strong; therefore, this is an overestimate of the actual background); (2) we estimated the background from the central 5′ of the PSPC in a set of deep observations and chose the highest; (3) no background subtraction. We found that the results of the fits (especially at energies higher than 0.5 keV) depend very little on the particular background adopted, since the background intensity is much smaller than the source intensity (between 3000 and 1800 counts in the 0.1–2.45 band and between 770 and 420 counts in the 0.5–2.45 band, depending on the background subtraction). The spectrum was compared to a thermal (Raymond & Smith 1977) model with metal abundances fixed at 0.3 (the value found by *Ginga*) and absorption fixed at the Galactic value of 0.9×10^{20} cm^{-2}. Therefore, only two parameters, the normalization and the temperature, are free to vary. In the following we present the results obtained with the background subtraction (2).

The fit to the Coma spectrum in the whole 0.1–2.45 energy band gives high reduced χ^2 both with the 1993 January (9.7) and with the 1992 March (5.7) matrices. Furthermore, the best-fit temperature is between 3 and 4 keV, significantly less than the value of about 8 keV found by *Ginga*. However, this simple model is probably inadequate in the complete energy band and cannot be used as a test for the resolution matrices. Reducing the energy band to 0.5–2.5 keV (channels 12–34) produces a big improvement in χ^2_r in the fit with both matrices: the fit with the 1993 January matrix is now completely acceptable ($\chi^2_r = 1.12$) and much better than the fit with the 1992 March matrix ($\chi^2_r = 2.74$). The residuals after the subtraction of the best-fit model from the Coma spectrum for the fit with the 1993 January matrix are shown in Figure 9, both as number of σ and as a fraction of the counts in each channel. The spectrum has been rebinned to enhance systematic deviations. No strong systematic feature is present in the residuals from the fit with the 1993 January matrix, and all deviations are the order of σ or less (2% of the source net counts or less), except for the point above 2 keV (where there is a positive deviation of 2 σ or 5% of the source counts). The best-fit temperature 6 ± 1 keV is lower than that found by *Ginga* (the best-fit temperature obtained with the 1992 March matrix is similar). We note that the field of view of the *Ginga* proportional counters is $2° \times 1°$ FWHM, much larger than the 5′ radius circle considered here, and therefore that the *Ginga* measurement is not dominated by gas at the center of the cluster, as is ours. It is possible that the spectrum of the inner region of the Coma Cluster is more complicated than a single-temperature thermal model with Galactic absorption, or that it is slightly cooler than the outer part. Fixing T at 8 keV (the temperature measured by *Ginga*) introduces a systematic wiggling in the residuals, but the deviations are always smaller than 2 σ or 5% of the source counts.

We conclude, therefore, that the magnitude of any residual systematic narrow features using the 1993 January matrix is certainly smaller than 5% and probably smaller than 2% of the source counts in the whole 0.5–2.5 keV energy range. To improve these limits, we need longer exposures or observations of brighter hard sources, which, to date, are not available in the *ROSAT* archive.

In the analysis presented in § 3 we included the standard flat systematic error of 1% suggested by Hasinger & Snowden (1992). While this is probably smaller than the real systematic error, it allows a more ready comparison of our results with those obtained in most previous *ROSAT* PSPC analyses. Furthermore, rather than inflating the errors, we prefer to inspect the deviations case by case: we considered only deviations of at least 5% of the counts per channel when discussing the reality of a spectral feature.

APPENDIX B

PSPC/IPC CROSS-CALIBRATION

We discuss here a comparison between PSPC and IPC spectra of a sample of sources. To avoid selection effects, we consider only one of the sources in the sample presented in this paper, MKN 205. In addition, we consider the bright radio-loud core-dominated quasar 3C 273 and the supernova remnant N132D. We extracted the IPC and PSPC spectra of 3C 273 and N132D and the IPC

TABLE 9

PSPC AND IPC OBSERVATIONS FOR CALIBRATION COMPARISON

Name	exposure[a]	net counts	Date	χ^2 (dof)[b]	χ^2 (dof)[c]
MKN205 PSPC	13891	13744 (3$\prime$)	1991Dec.-1992Apr.	67.4 (36)	32.6 (22)
IPC	13113	7050 (3$\prime$)	1980Apr.		
3C273 PSPC	6243	38015 (3$\prime$)	1991Dec.	135.1 (36)	48.0 (23)
IPC	1740	5121 (3$\prime$)	1979Jun.		
N132D PSPC	1110	11705 (5$\prime$)	1992Apr.	192.6 (36)	40.3 (22)
IPC	2929	9668 (5$\prime$)	1981Jan.		

[a] In seconds.
[b] PSPC channels 3–34; IPC channels 2–10.
[c] PSPC channels 3–21; IPC channels 2–10.

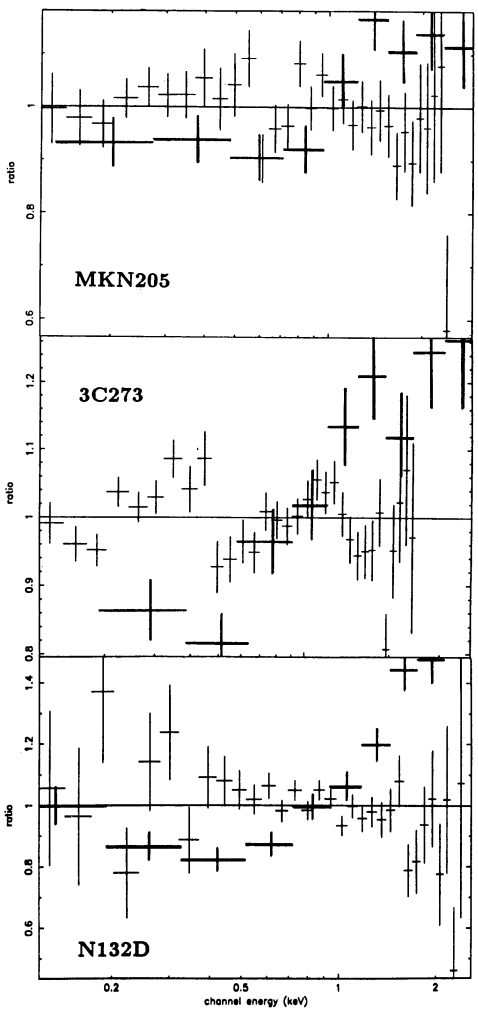

FIG. 10

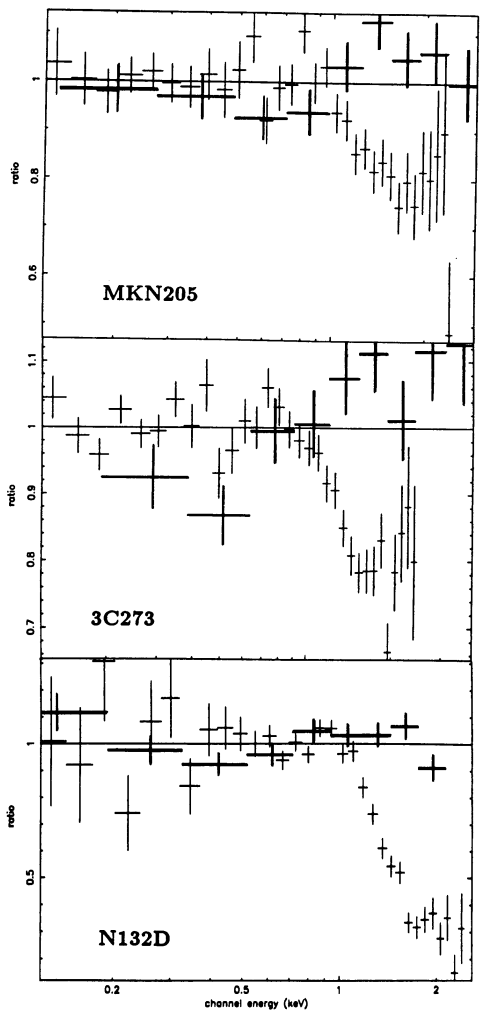

FIG. 11

FIG. 10.—The ratio between the observed and predicted counts in the two instruments for a broken power-law model (MKN 205 and 3C 273) and for a two-temperature Raymond-Smith model in the case of N132D. IPC points are identified by thicker lines.

FIG. 11.—The ratio between the observed and predicted counts in the two instruments for a broken power-law model (MKN 205 and 3C 273) and for a two-temperature Raymond-Smith model (N132D). The models are fitted to IPC channels 2–10 and to PSPC channels 3–21. The PSPC points not included in the fit are also shown. A large negative deviation is evident in these points.

spectrum of MKN 205 from the *Einstein* and *ROSAT* archives. Table 9 gives the exposure times and the net source counts in these observations. The three sources were observed by the PSPC-B after 1991 October 14.

We fitted the IPC and PSPC spectra (channels 2–10 and 3–34, respectively) simultaneously with several models, always letting the relative normalization be free to vary in the two instruments while requiring the other parameters to be the same in the two instruments. In the case of the two quasars, we also constrained the high-energy slope to be consistent with that found by *Ginga* (Williams et al. 1992). As an example, we plot in Figure 10 the ratio of the observed to the predicted counts in the two instruments for a broken PL model (MKN 205 and 3C 273) and for a two-temperature Raymond-Smith model (N132D). IPC points are identified by thicker lines. The χ^2 values are high (see Table 9), and the shape of the residuals is similar in the three cases, with a deficit of IPC counts below 1 keV and a large excess above this energy. The residuals obtained by fitting the other two or three component models are qualitatively similar to that in Figure 10. Also the residuals obtained by fitting these models to the other five quasars in the sample presented in this paper are similar to those in the figure. This shows that IPC spectra are systematically flatter than PSPC spectra (as suggested by Fig. 2 for a sample of 18 quasars).

We investigated this discrepancy further. First, we omitted parts of the PSPC spectrum from the fit. The best results were obtained by omitting the PSPC data above 1 keV. The results are given in Table 9 and shown in Figure 11, where we also plot the ratio of data to model for the PSPC points not included in the fit. A large negative deviation is evident in these points, suggesting a large overestimate of the predicted PSPC counts.

Alternatively, reasonably good fits can be obtained allowing at least one of the model parameters to be different in the two instruments. For example, good χ^2 values are obtained by allowing the parameter N_H to be free to vary independently. In all cases the IPC N_H was higher (by a factor 1.3–2).

Good χ^2 values can be also obtained by adding a narrow absorption feature, as an absorption edge, to the IPC model. The edge energy turns out to be consistent with that of the neutral oxygen edge at 0.54 keV. An edge at this energy is present in the PSPC response function, due to the oxygen present in the LEXAN coating of the PSPC window. The IPC has a similar LEXAN coating, but no edge is present in its response function, since a pure carbon window was assumed (Harnden et al. 1984). Introduction of an oxygen edge in the effective area curve of the IPC with an optical depth similar to that present in the PSPC helps, but it does not fully explain the discrepancy between the to instruments.

Further insight about whether the PSPC/IPC discrepancies are predominantly due to PSPC or IPC miscalibration could be obtained fitting simultaneously the data of these two instruments with that of the *Einstein* SSS or of the *ASCA* (*Astro D*) SIS, whose energy bands, at least partly, overlap with that of the PSPC and IPC. This is however, beyond the scope of the present investigation. We limit ourselves to conclude that to make full use of the high signal-to-noise ratio PSPC-IPC spectra, a major effort to study and possibly revise the relative PSPC-IPC calibration is needed.

REFERENCES

Allen, S. W., & Fabian, A. C. 1992, MNRAS, 258, 29P
Bahcall, J. N., Jannuzi, B. T., Schneider, D. P., Hartig, G. F., & Jenkins, E. B. 1992, ApJ, 398, 495
Barvainis, R. 1993, ApJ, 412, 513
Brunner, H., Friedrich, P., Zimmermann, H.-U., & Staubert R. 1992, X-Ray Emission from Active Galactic Nuclei and the Cosmic X-Ray Background, ed. W. Brinkmann & J. Trümper (MPE Report 235), 198
Comastri, A., Setti, G., Zamorani, G., Elvis, M., Giommi, P., Wilkes, B. J., & McDowell, J. C. M. 1992, ApJ, 384, 62
Elvis, M., Fassnacht, C., Wilson, A. S., & Briel, U. 1990, ApJ, 361, 459
Elvis, M., Fiore, F., Mathur, S., & Wilkes, B. J. 1994a, ApJ, 425, 103
Elvis, M., Fiore, F., Wilkes B. J., McDowell, J. C. M., & Bechtold, J. 1994b, ApJ, 422, 60
Elvis, M., Giommi, P., Wilkes, B. J., & McDowell, J. C. 1991, ApJ, 378, 537
Elvis, M., Green, R. F., Bechtold, J., Schmidt, M., Neugebauer, B. T., Soifer, B. T., Matthews, K., & Fabbiano, G. 1986, ApJ, 310, 291
Elvis, M., Lockman, F. J., & Wilkes, B. J. 1989, ApJ, 97, 777
Elvis, M., Wilkes, B. J., & Tananbaum, H. 1985, ApJ, 292, 357
Fiore, F., Elvis, M., Mathur, S., Wilkes, B. J., & McDowell, J. C. 1993, ApJ, 415, 129
Fiore, F., Elvis, E., Siemiginowska, A., Wilkes, B. J., McDowell, J. C., & Mathur, S. 1994, ApJ, submitted
Guilbert, P. W., & Rees, M. J. 1988, MNRAS, 233, 475
Harnden, F. R., Fabricant, D. G., Harris, D. E., & Schwarz J. 1984, SAO Special Rep. 393
Harris, D. E., et al. 1990, The Einstein Observatory Catalog of IPC X-Ray Sources CD-ROM, *Einstein* Data Center, Smithsonian Astrophys. Obs.
Hasinger, G., & Snowden, S. 1992, MPE note, II.1 PSPC Spectral Analysis
Hasinger, G., et al. 1992, Legacy, 2, 77 (OGIP Memo, Cal/ROS/92-001)
Jackson, N., Browne, I. W. A., & Warwick, R. S. 1993, A&A, 274, 79
Lampton, M., Margon, B., & Bowyer, S. 1976, ApJ, 208, 177
Laor, A., Fiore, F., Elvis, M., Wilkes, B. J., & McDowell, J. C. 1994, ApJ, in press
Lightman, A. P., & White, T. R. 1988, ApJ, 335, 57
Marscher, A. P. 1988, ApJ, 335, 552
Masnou, J.-L., Wilkes, B. J., Elvis, M., McDowell, J. C., & Arnaud, K. A. 1992, A&A, 253, 35
Morrison, R., & McCammon, D. A. 1983, ApJ, 270, 119
Nandra, K., & Pounds, K. A. 1992, Nature, 356, 215
Netzer, H. 1993, ApJ, 411, 594
Pan, H. C., Stewart, G. C., & Pounds, K. A. 1990, MNRAS, 242, 177
Perola, G. C., et al. 1986, ApJ, 306, 508
Pfefferman, E., et al. 1987, Proc. SPIE, 733, 519
Piro, L., Yamauchi, M., & Matsuoka, M. 1990, ApJ, 360, L35
Pounds, K. A., Nandra, K., Steward, G. C., George, I. M., & Fabian, A. C. 1990, Nature, 344, 132
Prestwich, A., McDowell, J. C. Plummer, D., Manning, K., & García, M. 1992, The *Einstein* Observatory Database of IPC Images in Event List Format, Smithsonian Inst. Astrophys. Obs.
Raymond, J. C., & Smith, B. W. 1977, ApJS, 35, 419
ROSAT Status Report., 1993, No. 64
Ross, R. R., & Fabian, A. C. 1993, MNRAS, 261, 74
Saxton, R. D., Turner, M. J. L., Williams, O. R., Stewart, G. C., Ohashi, T., & Kii, T. 1993 MNRAS, 262, 63
Schwartz, D. A., & Tucker, W. H. 1988, ApJ, 332, 157
Shastri, P., Wilkes, B. J., Elvis, M., & McDowell, J. C. 1993, ApJ, 410, 29
Stephan, K.-H., Shmitt, J. H. M. M., Snowden, S. L., Maier, H. J., & Frischke, D. 1991, Nucl. Meth. Instr. Phys. Res. A, 303, 196
Sulentic, J. W., & Arp, H. C. 1987, ApJ, 319, 687
Trinchieri, G., Kim, D. W., Fabbiano, G., & Canizares, P., 1994, ApJ, 428, 555
Trümper, J. 1983, Adv. Space Res., 2(4), 241
Turner, T. J. 1993, private communication
Turner, T. J., George, I. M., & Mushotzky, R. F. 1993a, ApJ, 412, 72
Turner, T. J., et al. 1993b, ApJ, 407, 556
Turner, T. J., Nandra, K., George, I. A., Fabian, A. C., & Pounds, K. A. 1993c, ApJ, 419, 127
Turner, T. J., & Pounds, K. A., 1988, MNRAS, 232, 463
———. 1989, MNRAS, 240, 833
Turner, T. J., Weaver, K. A., Mushotzky, R. F., Holt, S. S., & Madejsky, G. M. 1991, ApJ, 381, 85
Walter, R., & Fink, H. H. 1993, A&A, 274, 105
Wilson, A. S. Elvis, M., Lawrence, A., & Bland-Hawthorn, J. 1992, ApJ, 391, L75
Wilkes, B. J., & Elvis, M. 1987, ApJ, 323, 243
Williams, O. R., et al. 1992, ApJ, 389, 157
Yaqoob, T., & Warwick R. S. 1991, MNRAS, 248, 773